Lead exploration

1
2 Pharmacological evaluation
3

4
5 Structural characterization
6
7

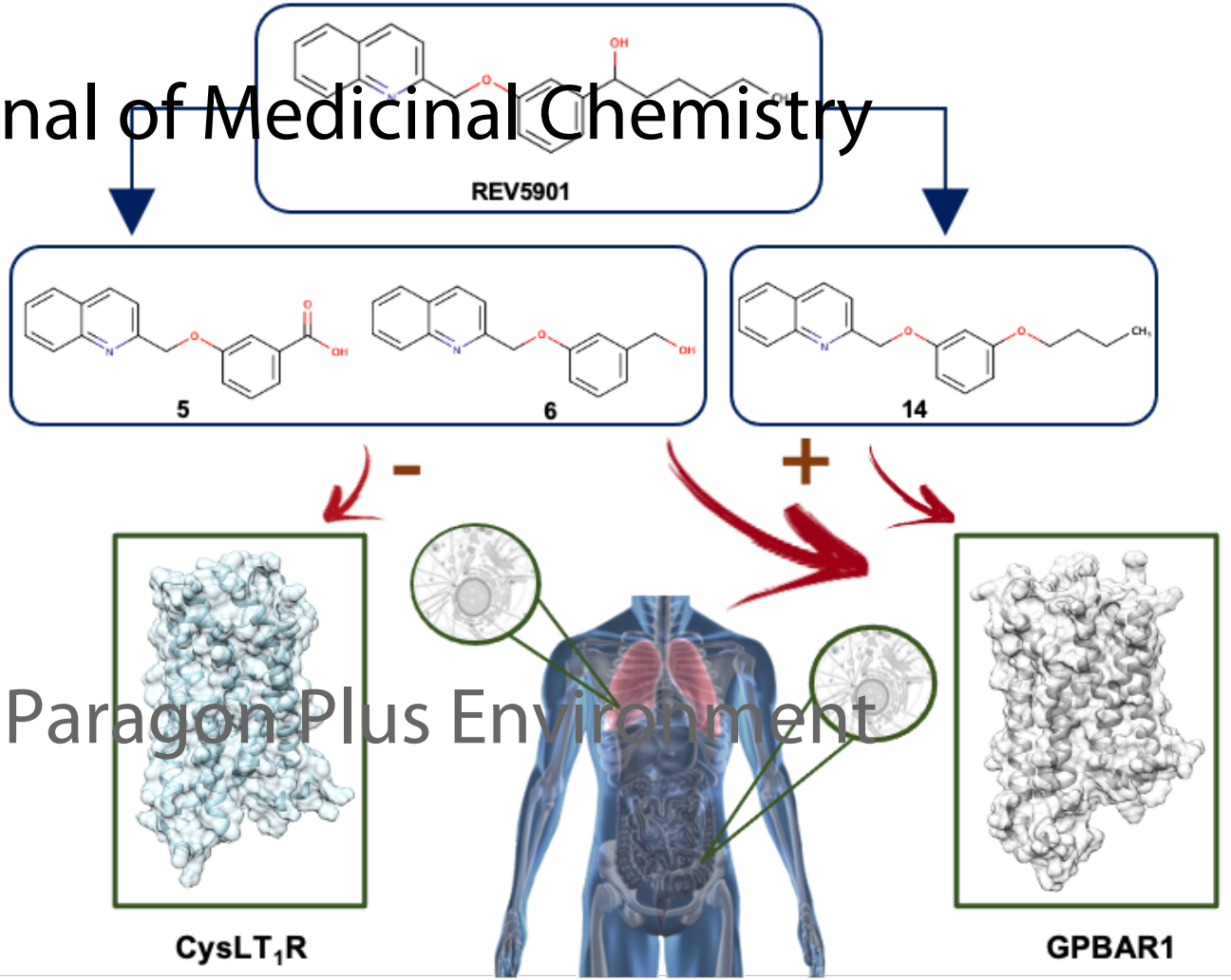

Structural basis for developing multitarget compounds acting on Cysteinyl Leukotriene Receptor 1 and G-Protein coupled Bile Acid Receptor 1

Bianca Fiorillo[1], Valentina Sepe[1], Paolo Conflitti[2], Rosalinda Roselli[1], Michele Biagioli[3], Silvia Marchianò[3], Pasquale De Luca[4], Giuliana Baronissi[1], Pasquale Rapacciuolo[1], Chiara Cassiano[1], Bruno Catalanotti[1], Angela Zampella[1], Vittorio Limongelli[1,2,*], Stefano Fiorucci[3]

[1]Department of Pharmacy, University of Naples "Federico II", Via D. Montesano, 49, I-80131 Naples, Italy

[2]Università della Svizzera italiana (USI), Faculty of Biomedical Sciences, Euler Institute, via G. Buffi 13, CH-6900 Lugano, Switzerland

[3]Department of Medicine and Surgery, University of Perugia, Piazza L. Severi 1-06132 Perugia, Italy

[4]Head – Sequencing and Molecular Analyses Center, RIMAR Stazione Zoologica, Villa Comunale, 80121 Naples, Italy

*To whom correspondence should be addressed. Tel.: +41 586664293 E-mail: vittoriolimongelli@gmail.com

Abstract.

G-Protein Coupled Receptors (GPCRs) are the molecular target of 40% of marketed drugs and the most investigated structures to develop novel therapeutics. Different members of the GPCRs superfamily can modulate the same cellular process acting on diverse pathways, thus representing an attracting opportunity to achieve multi-target drugs with synergic pharmacological effect. Here, we present a series of compounds with dual activity towards Cysteinyl Leukotriene Receptor 1 ($CysLT_1R$) and G-Protein coupled Bile Acid Receptor 1 (GPBAR1). They are derivatives of REV5901 - the first reported dual compound - with therapeutic potential in the treatment of colitis and other inflammatory processes. We report the binding mode of the most active compounds in the two GPCRs, revealing unprecedented structural basis for future drug design studies, including the presence of a polar group opportunely spaced from an aromatic ring in the ligand to interact with $Arg79^{2.60}$ of $CysLT_1R$ and achieve dual activity.

Introduction

Leukotriene receptors (LTR) are a pharmacologically relevant subfamily of class A G protein-coupled receptors (GPCRs) composed of five members: cysteinyl leukotriene receptor 1 ($CysLT_1R$) and 2 ($CysLT_2R$), leukotriene B4 receptor 1 (LTB4-R1) and 2 (LTB4-R2), and Oxoeicosanoid receptor 1 (OXER1). These receptors are activated by leukotrienes, which are eicosanoids derived from the oxidation of arachidonic acid acting as important mediators in inflammatory processes. In particular, the cysteinyl leukotrienes C4 (LTC_4), D4 (LTD_4) and E4 (LTE_4) are endogenous ligands of $CysLT_1R$ and $CysLT_2R$ with different potency and affinity (Figure 1).[1] Activation of CysLTRs by one of these molecules elicits cell responses through intracellular interaction with $G_{q/11}$ or $G_{i/o}$ proteins, which ultimately regulates cytokine secretion, vascular permeability, fibrosis, bronchoconstriction and recruitment of effector cells and mucus.[2,3,4,5,6,7] In particular, $CysLT_1R$ is known to mediate allergic and hypersensitivity reactions and when its signaling is exacerbated leads to pathological conditions as asthma and allergic rhinitis. $CysLT_1R$ is highly expressed in airway mucosal cells, in the lung smooth muscle, in bronchial fibroblasts and in different types of lung leukocytes, especially in asthmatic patients.[8,9] In addition, it is also present in the pancreas, small intestine, colon, liver and vascular endothelial cells.[10]

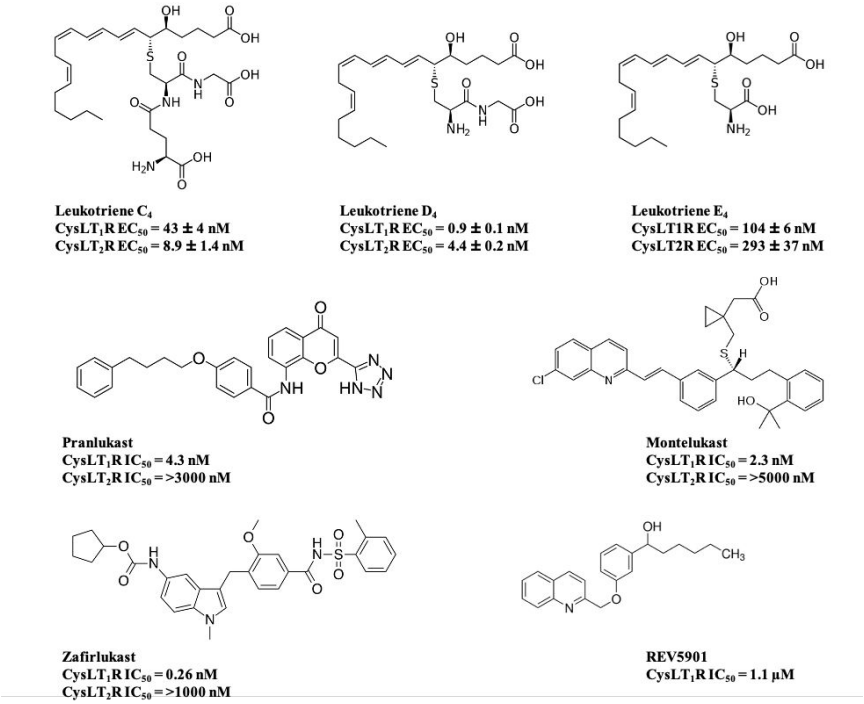

Figure 1. Endogenous ligands and previously reported $CysLT_1R$ antagonists.

The discovery of the first $CysLT_1R$ antagonists, namely montelukast, zafirlukast and pranlukast (Figure 1), has greatly impacted on the treatment of asthma and respiratory morbidities and many more $CysLT_1R$ antagonists have been developed and tested in preclinical and clinical trials.[3] Among these, we have recently reported alpha-pentyl-3-[2-quinolinylmethoxy] benzyl alcohol - REV5901 - (Figure 1) as the first compound endowed with dual activity as $CysLT_1R$ antagonist and agonist of the G protein-coupled bile acid receptor 1 (GPBAR1).[11] The latter is another class A GPCR activated by secondary bile acids and highly expressed in intestine, gallbladder, brown adipose tissue, muscles, and immune cells.[12,13,14,15] Targeting GPBAR1 with agonist molecules has demonstrated being a valid strategy to contrast hepatic inflammation, steatohepatitis, biliary diseases and metabolic syndromes.[16] In particular, we reported that REV5901 has positive effects in a mouse model of colitis with reduced levels of CysLTs, $CysLT_1R$, and cyclooxygenase 1 and 2 in a GPBAR1-dependant manner.[11] These data should be further analyzed considering that the $CysLT_1R$ antagonist montelukast has shown effect against colitis-associated colon carcinogenesis and inflammation.[17] Therefore, compounds acting as $CysLT_1R$ antagonists and GPBAR1 agonists are

expected to exert broad anti-inflammatory effects by modulating multiple molecular targets including cytokines and chemokines expression, macrophages migration, vasodilatation, monocytes differentiation and cell proliferation.[18,19]

The discovery of dual $CysLT_1R$ antagonists/GPBAR1 agonists is of great demand and the recent release of the X-ray structures of $CysLT_1R$ (PDB ID 6rz4 and 6rz5)[20] and cryo-EM structures of GPBAR1 (PDB ID 7cfn and 7bw0)[21,22] paves the way to structure-based drug design studies. With this aim, we have investigated REV5901 as lead compound to develop a series of non-steroidal ligands endowed simultaneously with $CysLT_1R$ antagonist and GPBAR1 agonist activity. We explored a number of modifications of the REV5901's quinoline scaffold identifying two compounds, **5** and **6**, with potent dual-target activity and one ligand, **14**, with selective activity towards GPBAR1. Then, we investigated through advanced molecular binding simulations the interaction of compounds **5**, **6** and **14** with $CysLT_1R$ and GPBAR1, which allowed disclosing the ligand binding mode and the key molecular interactions established in the two receptors' binding site. Finally, in vitro pharmacokinetics properties of compounds **5**, **6** and **14** were determined, thus deploying the newly designed compounds in a privileged position to enter preclinical studies.

Our study reports novel $CysLT_1R$/GPBAR1 dual-target and selective GPBAR1 compounds and provides the structural basis to achieve ligands endowed with simultaneous modulation of $CysLT_1R$ and GPBAR1. This represents an unprecedented knowledge for these two important GPCR receptors, a stepping-stone towards the design of $CysLT_1R$/GPBAR1 dual ligands as drug candidates against inflammation, metabolic syndromes and other $CysLT_1R$/GPBAR1 related diseases.

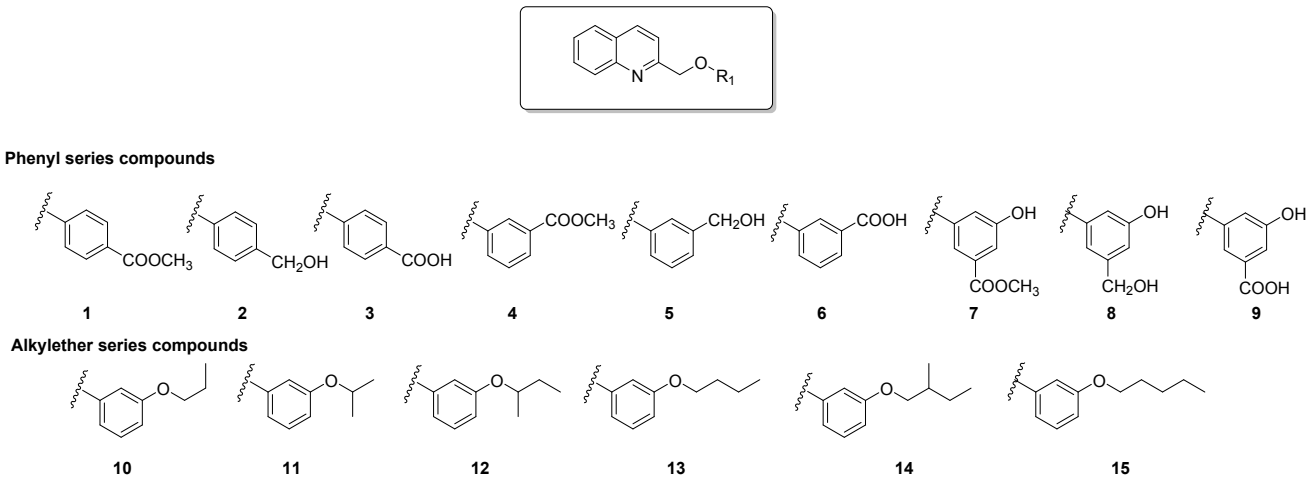

Figure 2. Chemical structure of derivatives **1–15** identified in this study.

Results

Chemical Synthesis. REV5901 chemical scaffold was modified in the secondary alcoholic alkyl side chain on the quinoline scaffold with the aim of obtaining novel, more potent ligands endowed with agonistic and antagonistic activity towards GPBAR and $CysLT_1R$, respectively and with better pharmacokinetic profiles. As such, we have designed a series of phenoxy-methyl-quinoline derivatives (Figure 2) by introducing on the benzene ring some polar substitutions (compounds **1-9**), or alkylether decoration to mimicking the side chain of REV5901 (compounds **10-15**).

As depicted in the Scheme 1, the synthesis of compounds **1-6** started with the ester reduction via DIBAL-H solution of the commercially available methyl quinoline-2-carboxylate (**16**) and the subsequent Mitsunobu reactions with two different phenols (methyl 4-hydroxybenzoate or methyl 3-hydroxybenzoate) to produce compounds **1** (76% yield) and **4** (78% yield), respectively. Basic hydrolysis and DIBAL-H reduction on methyl esters furnished the corresponding alcohols **2** (68% yield) and **5** (60% yield) and the carboxylic acids **3** (43% yield) and **6** (68% yield).

Scheme 1. Synthesis of compounds 1-6.[a]

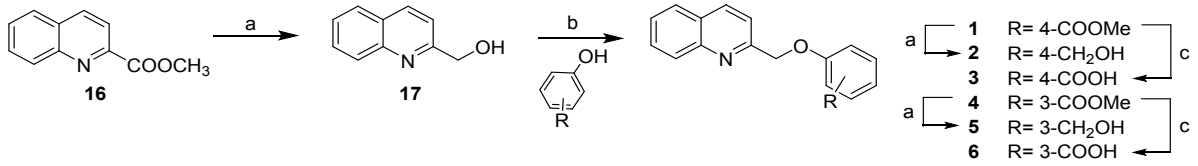

[a]*Reagents and Conditions*. a) DIBAL-H, THF dry, 0°C; b) PPh_3, DIAD, THF dry, 0° C, 76% and 78% yield respectively; c) NaOH, MeOH: H_2O 1:1 v/v, 43% and 68%, respectively.

The synthesis was completed in a total of two or three steps starting from commercially available **16** and was found to proceed with a good total yield that oscillates between 72 and 31%.

Derivative **17** was also used as starting material to obtain compounds **7-9**, as described in Scheme 2. In this case, Williamson ether synthesis starting from mesylate derivative of alcohol **17** and alcohol **19**, previously prepared by monoprotection of methyl 3,5-dihydroxybenzoate, produced compound **21**. Finally, TBS deprotection (85% yield), DIBAL-H reduction and basic hydrolysis furnished compounds **7** (85%), **8** (92%) and **9** (quantitative yield), respectively.

Scheme 2. Synthesis of compounds 7-9.[a]

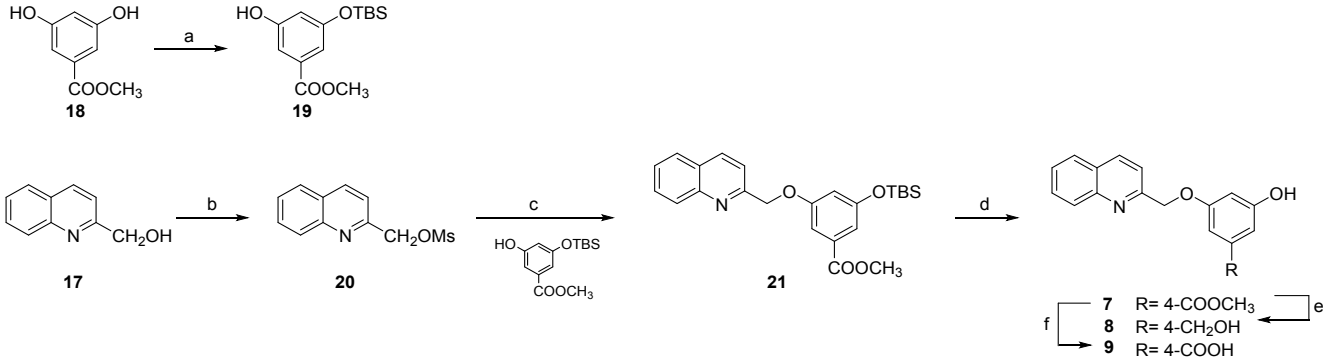

[a]*Reagents and Conditions*. a) TBS-Cl, imidazole, dry DMF, 50%; b) MsCl, dry TEA, dry diethylether, -20°C, 85%; c) compound **19**, K_2CO_3, dry DMF, 100°C, 87%; d) TBAF 1.0 M in dry THF, over-night, 85%; e) DIBAL-H, dry THF, 0°C, 92%; f) NaOH in excess, MeOH:H_2O 1:1 v/v, reflux, quantitative yield.

Finally, in order to increase the chemical space and investigate the structural requisites for dual GPBAR1/$CysLT_1R$ modulation, we developed a series of quinoline derivatives modifying aromatic ring in the length of alkyloxy-side chain (compounds **10-15**). The key intermediate mesylate **20** was utilized in multiple Williamson reactions with six different phenols, previously synthesized through

a multi-step procedure, involving TBS protection of resorcinol, Mitsunobu reactions with various alcohols, and TBS deprotection (scheme 3, intermediates **24-29**).

Scheme 3. Synthesis of alkylether derivatives.[a]

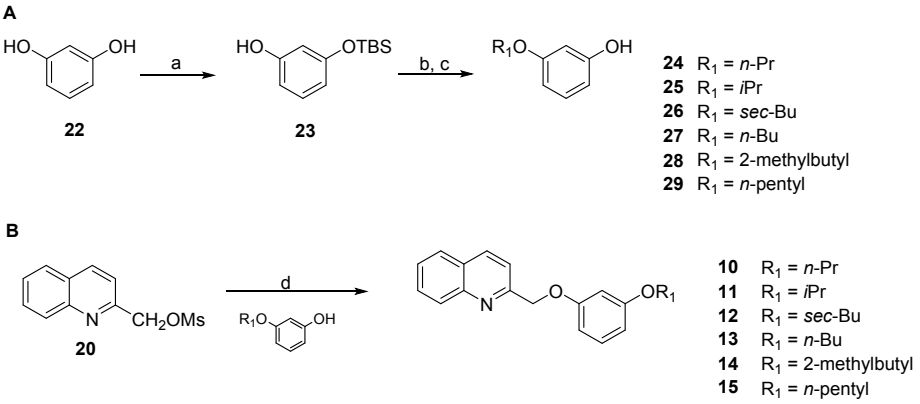

[a]*Reagents and Conditions*. a) TBS-Cl, imidazole, dry DMF, 47%; b) PPh_3, DIAD, alcohols, THF dry, 0° C; c) TBAF 1.0 M in THF dry, over-night, 47-84% yield over two steps; d) compounds **24-29**, K_2CO_3, DMF dry, 100°C, 61%-quantitative yield.

Pharmacological evaluation. Derivatives **1-15** were tested for GPBAR1 agonistic activity, in a luciferase reporter assay with HEK-293T cells transfected with GPBAR1, respectively. Evaluation of the antagonist activity of compounds at the human $CysLT_1$ receptor expressed in transfected CHO cells was determined by measuring their effect on agonist-induced cytosolic Ca^{2+} ion mobilization using a fluorimetric detection method.[23] Cellular antagonist effect was calculated as a % inhibition of control reference agonist (LTD_4) response for each target.

Agonistic activity of compounds on GPBAR1 was compared to that of the reference compound TLCA, which was set as 100%. As shown in Table 1, the best results in terms of efficacy and potency on the receptors are found in compounds **5** and **6**, as dual modulators and in compound **14** as GPBAR1 agonist.

We investigated whether the compounds could exert an in vitro anti-inflammatory activity. For this purpose, mouse RAW264.7 macrophages were primed with LPS (lipopolysaccharide), and co-incubated with or without compounds 5, 6 or 14 at 0.1, 1.5 and 10 μM.

Table 1. Efficacy and potency for compounds **1-15**.

Compounds of formula	**CysLT$_1$R**[a]	**IC$_{50}$**[b] (μM)	**GPBAR1**[c]	**EC$_{50}$**[d] (μM)
REV5901	116.80 ± 0.21	1.10 ± 0.50	136.74 ± 27.80	2.50 ± 1.20
1	48 ± 4.60	nd	20.70 ± 8.45	nd
2	85 ± 3.32	2.10 ± 1.50	12.63 ± 4.11	nd
3	-11 ± 4.38	nd	32.15 ± 3.29	16.50 ± 0.71
4	85 ± 0.91	3.90 ± 1.50	23 ± 4.76	nd
5	97 ± 0.78	1.20 ± 0.42	92.69 ± 0.73	7.40 ± 1.84
6	71 ± 2.05	2.80 ± 0.38	74.80 ± 3.96	3 ± 0.30
7	59 ± 3.25	nd	17.58 ± 1.37	nd
8	26 ± 14.30	nd	72.92 ± 1.57	23 ± 1.41
9	3 ± 7.42	nd	29.80 ± 0.89	20 ± 0.71
10	66 ± 4.66	5.11 ± 1.6	112.34 ± 12.21	1 ± 0.04
11	79 ± 5.09	nd	14.99 ± 1.81	nd
12	66 ± 0.07	9.63 ± 1.3	100.50 ± 13.91*	0.1 ± 0.05
13	4 ± 8.27	nd	138.88 ± 11.15	0.50 ± 0.22
14	15 ± 3.67	nd	106.43 ± 4.45	0.17 ± 0.07
15	22 ± 4.38	nd	137 ± 12.93	1.80 ± 0.07

[a]These assays were performed by Eurofins Cerep-Panlabs (France). The results are expressed as a percent inhibition of the control response to 0.1 nM LTD4. The standard reference antagonist is MK 571. Results are mean of two experiments ±SD.
[b]Results are mean of at least two experiments ±SD and IC$_{50}$ was determined for efficacy>60%. .
[c]Eff (%) is the maximum efficacy of the compound (10 μM) relative to TLCA (10 μM) as 100 in transactivation of a cAMP responsive element (CRE) on HEK293T cells; results are mean of two experiments ±SD.
[d]Results are mean of at least two experiments ±SD and EC$_{50}$ was determined for efficacy>25%.
*Efficacy calculated with 1 μM of compound.
nd, not determined.

As shown in Figure 3, all compounds reduced the production of pro-inflammatory cytokines (Tnfα and Il-1β) induced by the LPS, but additionally only **5** and **14** increased the expression of the anti-inflammatory gene Il-10. In the same experimental set, we also tested the REV5901. As shown in Figure S1, the effects exerted by REV501 were similar to those exerted by the new compounds. Indeed REV501 blunted the expression of pro-inflammatory cytokines in macrophages exposed to LPS while induced the expression of Il-10 (Figure S1).

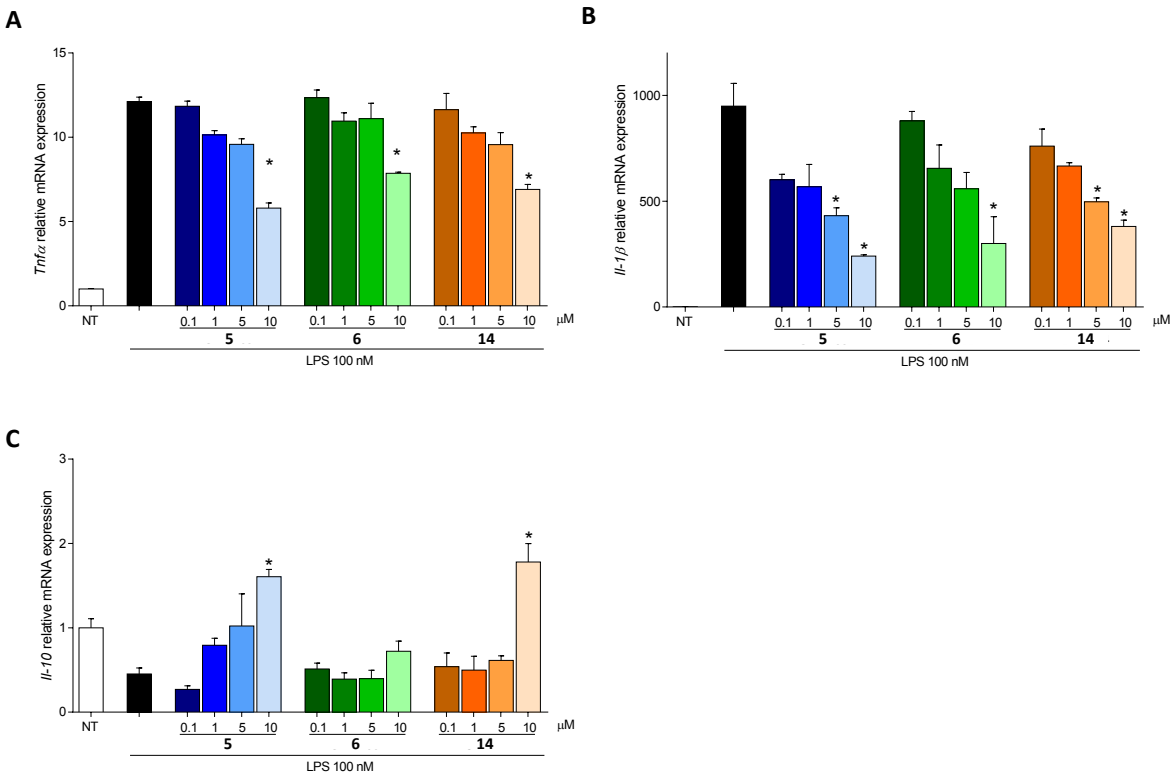

Figure 3. RAW264.7 cells were classically activated with LPS (100 nM) and exposed or not to compounds **5**, **6** or **14** at the concentration of 0.1, 1.5 and 10 μM for 16 h. Quantitative real-time PCR analysis of expression of pro-inflammatory genes Tnf-α (**A**) and Il-1β (**B**), and anti-inflammatory genes Il-10 (**C**). These data are normalized to Gapdh/18s mRNA. Data are derived from 6 replicates from 2 independent experiments. Results represent the mean ± SEM. *$p < 0.05$ vs LPS group. Anova-way analysis of variance was used for statistical comparisons.

In order to further characterize the pharmacological profile of the novel derivatives, we have investigated whether compounds **5**, **6** and **14** modulate the RAW264.7 proliferation induced by LTD4. As shown in Figure 4, REV5901 was used as control.

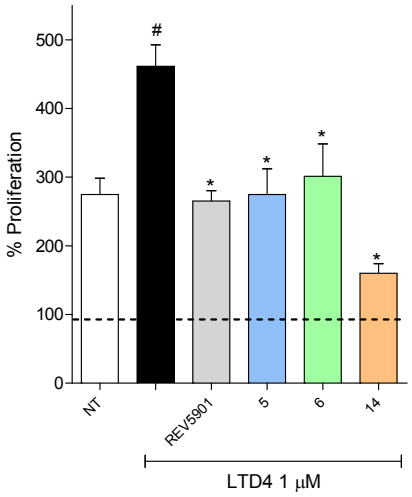

Figure 4. RAW264.7 were exposed to LTD4 (1 μM) for 48 h alone or in combination with compounds at concentration of 10 μM. Cell counting was performed using Trypan Blu staining. Data are derived from 6 replicates from 2 independent experiments. Results represent the mean ± SEM. #$p < 0.05$ vs NT group and *$p < 0.05$ vs LTD4 group. Anova-way analysis of variance was used for statistical comparisons.

For these experiments we used again RAW264.7 cells. The results of these experiments demonstrated that while LTD4 increases RAW264.7 cells proliferation (the number of cells approximately tripled by 48 h in absence of stimulus, but increased by 5 folds in the presence of LTD4) (Figure 4), compound **5**, **6** and **14**, and REV5901 reversed this effect, confirming the concept that the three compounds act as CysLTR1 antagonist (Figure 4).

We have previously shown that GPBAR1 regulates the expression of adhesion molecules endothelial and immune cells and therefore attenuates the influx of immune cells from the circulation into the inflamed tissues.[24,25,26,27] An important role in this process is also contributed by leukotrienes which promote cell adhesion and leukocyte rolling.[28,29,30,31] For these reasons, we have also tested the efficacy of novel compounds in an adhesion assay, using human aortic endothelial cells (HAEC cells) and a human monocytic cell line (U937 cells) (Figure 5).

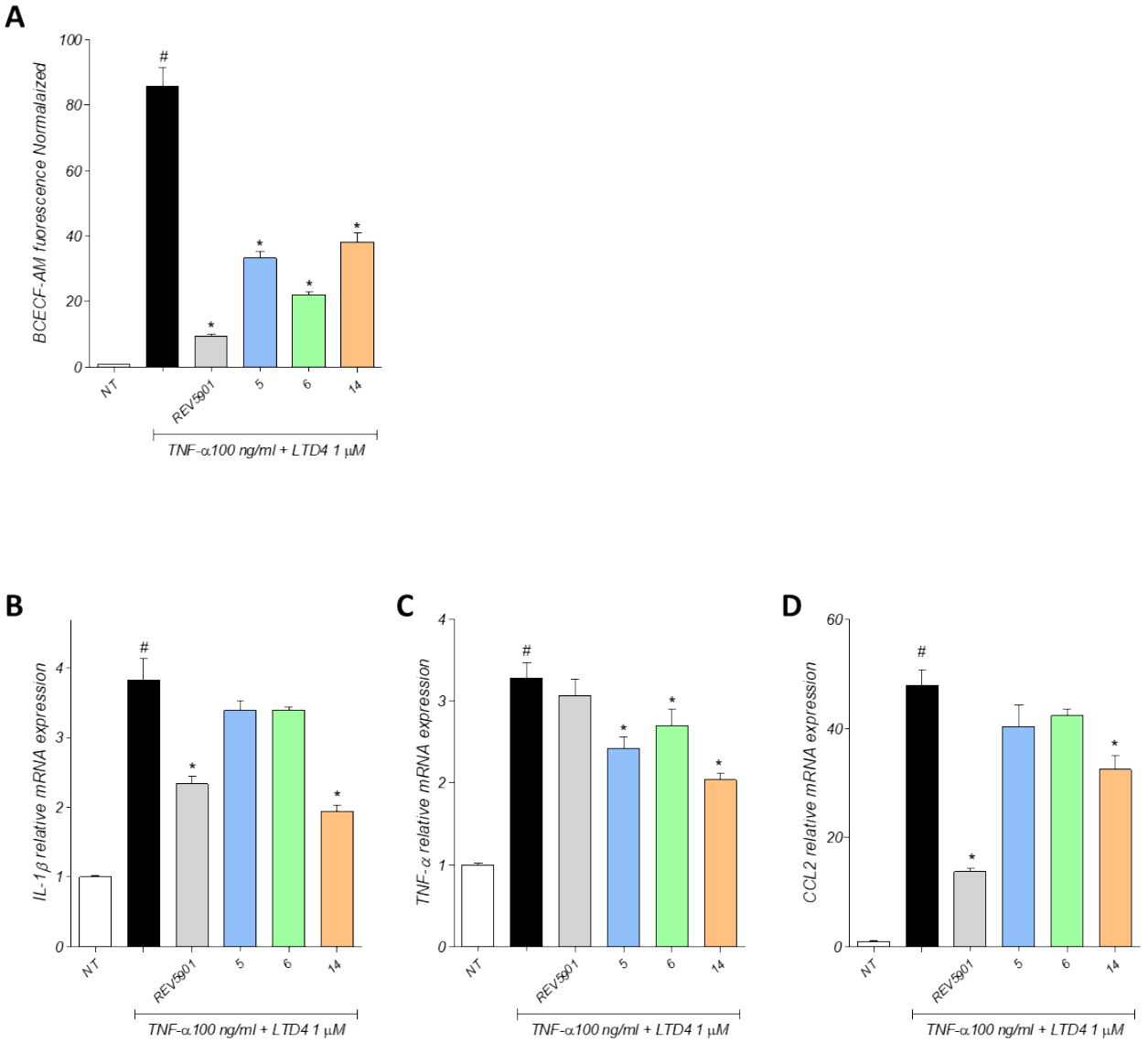

Figure 5. HAEC cells were plated on a 24-well plate and activated with TNFα (100 ng/mL) and LTD4 (1 μM) for 24 h alone or in combination with compounds **5**, **6**, **14** and REV5901 at 10 μM. U937 cells were treated under the same conditions. (**A**) For adhesion assay, U937 cells were fluorescently labeled with BCECF-AM and were incubated for 120 min with HAEC cells. Nonadherent monocytes were removed by gentle washing and fluorescence intensity was measured (485-nm excitation and 520–560-nm emission) using a microplate reader. (**B**) Quantitative real-time PCR analysis of expression of pro-inflammatory genes Il-1β (**B**) and Tnf-α (**C**) and chemokine Ccl2 (**D**) in U937 cells. These data are normalized to Gapdh mRNA. Data are derived from 8 replicates from 2 independent experiments. Results represent the mean ± SEM. #$p < 0.05$ vs NT group and *$p < 0.05$ vs TNF-α + LTD4 group. Anova-way analysis of variance was used for statistical comparisons.

The results shown in Figure 5 demonstrated that exposure of cells to TNF-α + LTD4 increases the adhesion of monocytes to HAEC by approximately 100-fold (Figure 5A). All the tested compounds, **5**, **6**, **14** and REV5901, significantly reduced the adhesion of U937 cells to HAEC. Since cell-to-cell adhesion in this assay results in monocytes activation, we have measured the expression of additional mediators, i.e., IL-1β and TNF-α, and CCL2 produced by U937 cells (Figures 5B-D). The data shown in Figure 5B-D demonstrated that exposure of cells to TNF-α + LTD4 increased expression of these mediators and that all tested compounds reversed this effect. Compound **5** and **6** reduced the expression of TNF-α to a larger extent than REV5901 (Figure 5C), but were less effective on IL-1β and CCL2 (Figure 5B-D). Interestingly, compound **14** was the most effective compound, down-regulating at a larger extent the expression of these inflammatory genes (Figures 5B-D).

Structural studies. Molecular docking calculations were performed to investigate the binding modes of compounds **1-15** to $CysLT_1R$ and GPBAR1[32,33,34,35] using the Glide software package (see Methods for details).[36,37] As regards the docking simulations in $CysLT_1R$, the crystallographic structure with PDB ID 6rz4[20] has been employed, while for GPBAR1, we used both the cryo-EM structures (PDB ID 7cfn and 7bw0)[21,22] and the 3D model developed in-house[38] that has already been successfully employed in numerous drug design studies[39,40,41] (see Methods for details).

Docking calculations of **1-15** in the GPBAR1 model showed remarkably similar binding modes, with the quinoline group positioned in the amphipathic pocket between transmembrane helices (TM) 3 and 5, interacting with residues known to participate to ligand/GPBAR1 binding like $Tyr89^{3.29}$, $Asn93^{3.33}$, $Phe96^{3.36}$ and $Trp237^{6.48}$ (superscripts refer to Ballesteros-Weinstein numbering) (e.g., see Figure 6).[11,38,40,41,42,43] On the other hand, docking calculations in the cryo-EM structures did not lead to convergent results, either involving residues known to contribute to ligand binding, therefore they were not further considered in the study. In $CysLT_1R$, compounds **1-**

15 showed similar binding modes where the quinoline moiety is placed in the pocket formed by TM3, TM4 and TM5, directed towards the bilayer-embedded lateral entrance of the receptor[11] (e.g., see Figure 6). Therefore, the docking results show a propensity of the quinoline scaffold to bind promiscuously both $CysLT_1R$ and GPBAR1. Thus, we decided to further investigate the binding mode of compounds **5** and **6**, the most potent $CysLT_1R$/GPBAR1 dual ligands, and compound **14**, which is a selective GPBAR1 ligand, with the scope to elucidate the structural basis for $CysLT_1R$/GPBAR1 dual modulation.

Binding mode of 5 in GPBAR1. Compound **5** is the most potent dual-target ligand of the series. The most populated binding mode in GPBAR1 shows the quinoline scaffold anchored between TM3 and TM5, forming a H-bond with Asn93$^{3.33}$ and hydrophobic interactions with Phe96$^{3.36}$,[44] Leu97$^{3.37}$, Leu100$^{3.40}$, Leu173$^{5.46}$ and Leu174$^{5.47}$ (Figure 6A). Furthermore, the phenyl group makes polar and apolar contacts with Leu71$^{2.60}$, Tyr89$^{3.29}$, Pro92$^{3.32}$, Glu169$^{5.42}$, Trp237$^{6.48}$ and Leu266$^{7.39}$. Finally, the methyl-hydroxyl group extends towards TM1 and TM7, pointing towards Leu68$^{2.57}$ and forming an additional H-bond interaction with Ser270$^{7.43}$. The docking binding mode was validated by means of atomistic molecular dynamics (MD) calculations where the stability of the binding mode was investigated simulating the receptor flexibility and the solvent effect, which are important factors in ligand binding typically neglected by docking calculations.[45] Along the MD simulation, the ligand assumes a stable binding mode - very similar to the docking pose - that is preserved until the end of the calculation, as shown by the values of the root mean square deviation (RMSD) computed on the ligand heavy atoms (Figure 8C). In more detail, conformational cluster analysis of the ligand binding poses visited during the MD resulted in one single cluster, with its centroid depicted in Figure 8A (see Methods for details). In this pose, the quinoline scaffold is located between TM3 and TM5, where interacts with residues such as Tyr89$^{3.29}$, Leu97$^{3.37}$, Glu169$^{5.43}$, Leu173$^{5.46}$, and Leu244$^{6.55}$. As seen in the docking pose, the quinoline moiety H-bonds with Ans93$^{3.33}$, whereas it forms a π-π stacking interaction with Phe96$^{3.36}$. The phenyl group of **5** engages a T-shaped π stacking interaction with Trp237$^{6.48}$ and extending through the binding site

cavity it also interacts with Leu68$^{2.57}$, Leu71$^{2.60}$, Thr74$^{2.63}$, Pro92$^{3.32}$ and Leu266$^{7.39}$. This pose is further stabilized by the two H-bonds formed between the ligand terminal hydroxyl group and Ser270$^{7.43}$, and by the ligand ethereal oxygen and Tyr240$^{6.51}$.

Binding mode of 5 in CysLT$_1$R. In CysLT$_1$R, the quinoline group of **5** is oriented orthogonal to TM3 and TM5 and occupies the pocket formed by Tyr108$^{3.37}$, Ser155$^{4.57}$, Phe158$^{4.60}$, Val186$^{5.35}$, Ser193$^{5.42}$ and Leu257$^{6.59}$ (Figure 6B). The ligand binding pose is stabilized by the cation-π interaction formed by the quinoline moiety with Arg253$^{6.55}$ and the H-bond between the ligand's ethereal oxygen and Tyr104$^{3.33}$. The latter residue and Tyr249$^{6.51}$ also form T-shaped π stacking interactions with the phenyl ring of **5** that contribute to further stabilize the binding mode. It is interesting to note that the binding mode of **5** resembles the crystallographic binding pose of the known CysLT$_1$R antagonist pranlukast[19] with a similar occupation of the receptor binding site (Figure 7). Upon a closer visual inspection, one might find that pranlukast interacts through its tetrazole group with Arg79$^{2.60}$ via a direct and a water-mediated interaction, and such interaction might be emulated by compound **5** with its terminal hydroxyl group point towards Arg79$^{2.60}$, Val277$^{7.35}$ and Leu281$^{7.39}$ (Figure 6B and Figure 7). However, water molecules are not explicitly considered in docking simulations and to take this aspect into account a deeper investigation of the binding interaction of **5** with CysLT$_1$R is required. This was performed by means of molecular dynamics (MD) and free-energy calculations where the ligand and receptor conformational flexibility was fully taken into account and the solvent effect was simulated by the presence of explicit water molecules in the binding cavity. The results are discussed in the following section.

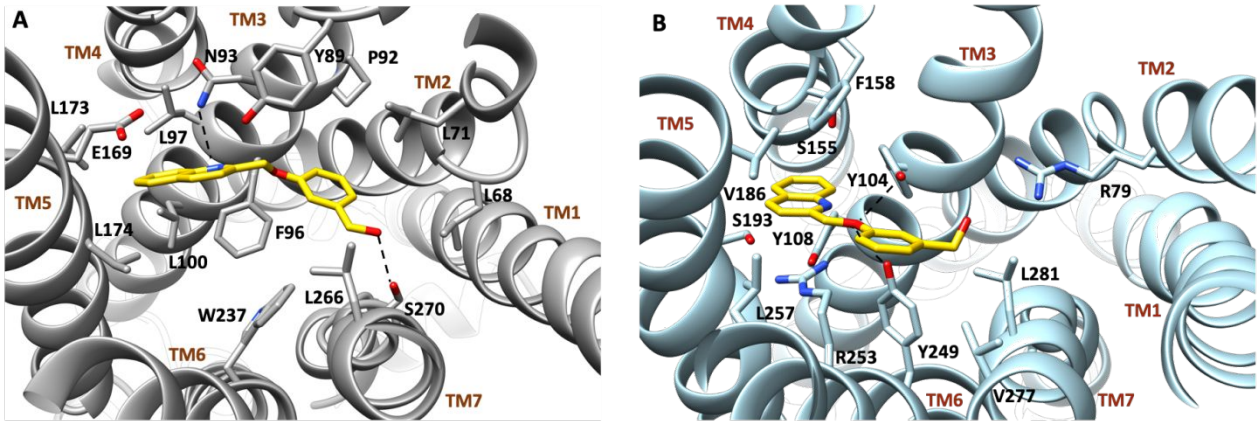

Figure 6. Binding modes of **5** in (**A**) GPBAR1 and (**B**) $CysLT_1R$ identified via docking calculations. The ligand is represented as gold sticks, whereas the interacting residues of the receptors are shown in grey (GPBAR1) or cyan ($CysLT_1R$) and labelled. Oxygen atoms are depicted in red and nitrogen atoms in blue. The receptors are represented as grey (GPBAR1) or cyan ($CysLT_1R$) ribbons with their TMs labelled. Hydrogens are omitted for the sake of clarity and H-bonds are displayed as black dashed lines.

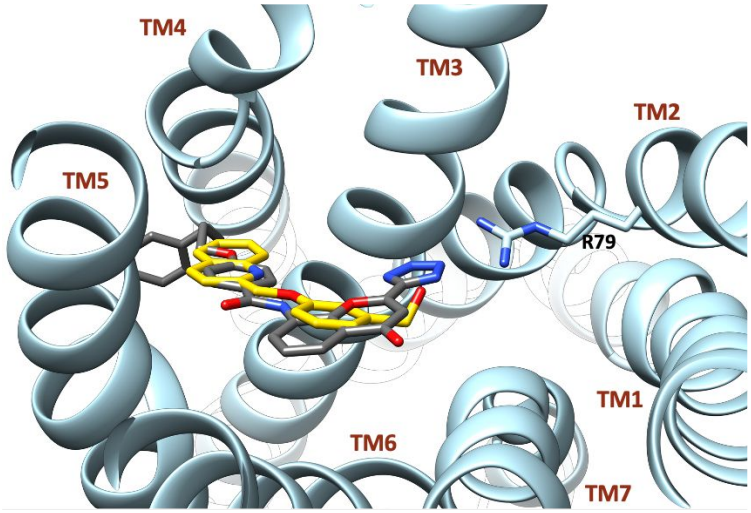

Figure 7. Comparison between the binding mode of **5** (gold sticks) and pranlukast (grey sticks) to $CysLT_1R$. Oxygen atoms are depicted in red and nitrogen atoms in blue. The receptor is represented as cyan ribbons with its TM and H labelled. $Arg79^{2.60}$ is shown in cyan sticks. Hydrogens are omitted for the sake of clarity.

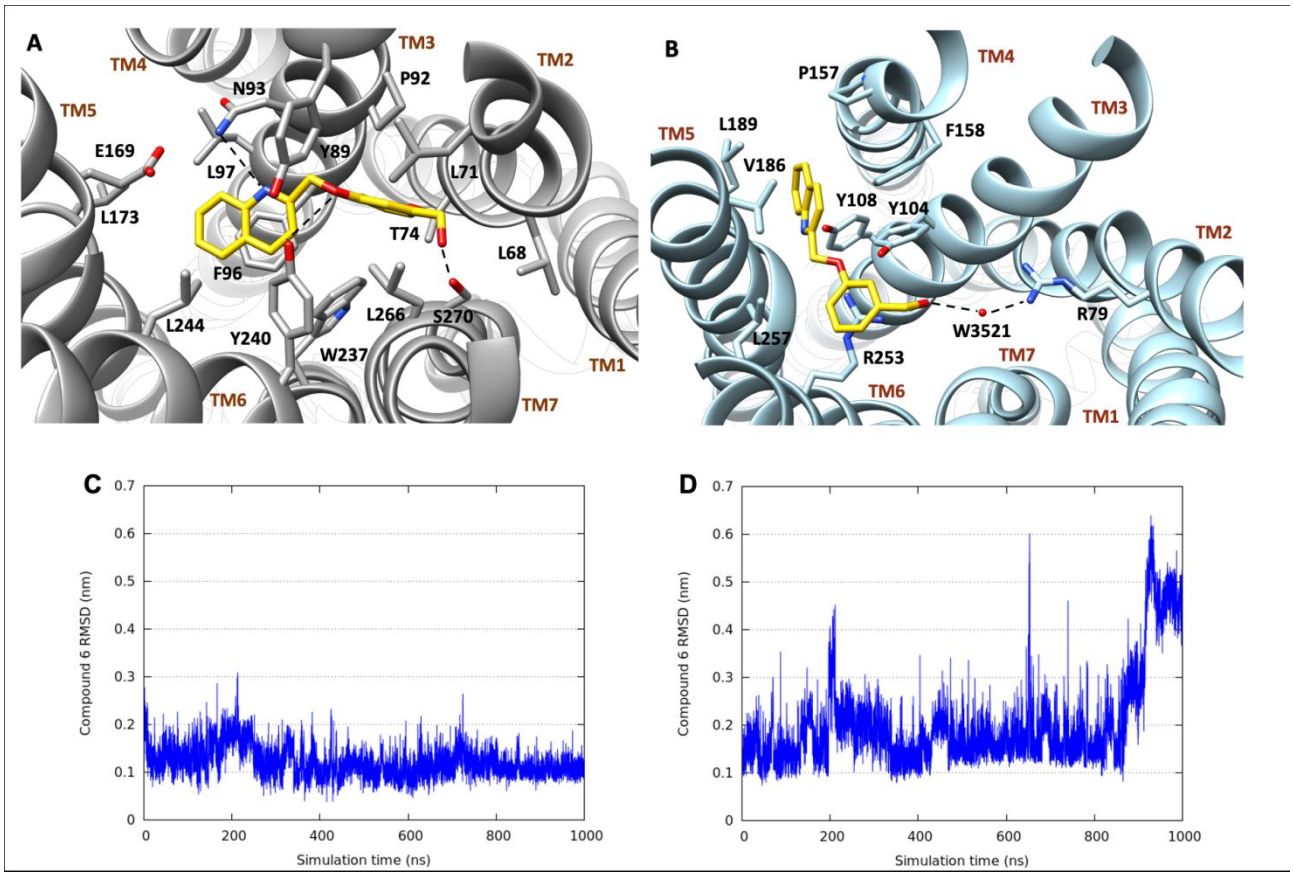

Figure 8. A-B) Centroids of the most populated clusters of **5** in (**A**) GPBAR1 and (**B**) $CysLT_1R$ MD simulations. The ligand is represented as gold sticks, whereas the interacting residues of the receptors are shown in grey (GPBAR1) or cyan ($CysLT_1R$) and labelled. Oxygen atoms are depicted in red and nitrogen atoms in blue. The receptors are represented as grey (GPBAR1) or cyan ($CysLT_1R$) ribbons with their TMs labelled. Hydrogen atoms are omitted for the sake of clarity and H-bonds and salt bridges are displayed as black dashed lines; **C-D**) Average RMSD of the heavy atoms of **5** in GPBAR1 (**C**) and $CysLT_1R$ (**D**) along the MD simulations. Prior to the RMSD calculations, trajectory frames were aligned on the same atoms.

MD and free-energy calculations. During 1 μs MD simulation, the binding mode of **5** in $CysLT_1R$ is stable, however, showing a slight flexibility in the methyl-hydroxyl terminal group in the last 100 ns (Figure 8D). This motion allows a water molecule to mediate optimally a H-bond between **5** hydroxyl group and $Arg79^{2.60}$, as shown in the most populated binding pose during the MD (Figure 8B). Here, the quinoline scaffold is placed between TM4 and TM5, where it forms contacts with $Tyr108^{3.37}$, $Pro157^{4.59}$, $Val186^{5.35}$, $Leu189^{5.38}$ and a T-shaped π stacking interaction with $Phe158^{4.60}$.

On the other hand, the phenyl ring interacts with Tyr104$^{3.33}$, Leu257$^{6.59}$ and engages in a cation- π interaction with Arg253$^{6.55}$. We note that the MD binding mode slightly differs from the docking pose, particularly in the positioning of the quinoline ring between TM4 and TM5 and the reorientation of the methyl-hydroxyl tail that makes room for the water molecule mediating the H-bond interaction with Arg79$^{2.60}$ (Figure 6B and 8B). As previously introduced, a similar interaction is engaged by the antagonist pranlukast in the receptor binding site. Considering the difference between the MD and the docking pose, we decided to investigate more deeply the binding of **5** in $CysLT_1R$ using a more accurate methodology based on free-energy calculations. In particular, we performed metadynamics calculations (MetaD),[46,47] which is an advanced technique successfully employed by us and other groups to disclose ligand binding mode in several DNA and protein systems including GPCRs[45,48,49,50,51,52]. Briefly, the method consists in adding a Gaussian potential on user-defined degrees of freedom - named Collective Variables (CVs) - of the system under investigation. In doing so, the system explores the free energy landscape, passing from one energy minimum to another. At the end of the calculation, the ligand binding mode is identified as the lowest energy minimum. In our case, in order to describe the binding of **5** to the $CysLT_1R$ binding pocket, we defined as CV the distance between the center of mass of the ligand's quinoline ring and the C_β of Arg79$^{2.60}$. As shown by the computed free energy profile reported in Figure 7A, we found the lowest energy minimum at 1.8 nm. Here, the ligand binding mode is strikingly similar to the MD pose with a remarkably low RMSD value of 0.08 nm computed for the ligand heavy atoms (Figure 9B). This finding confirms and supports the MD binding mode, especially considering that during the MetaD simulation the ligand is free to move in the binding site, exploring all the possible binding modes.

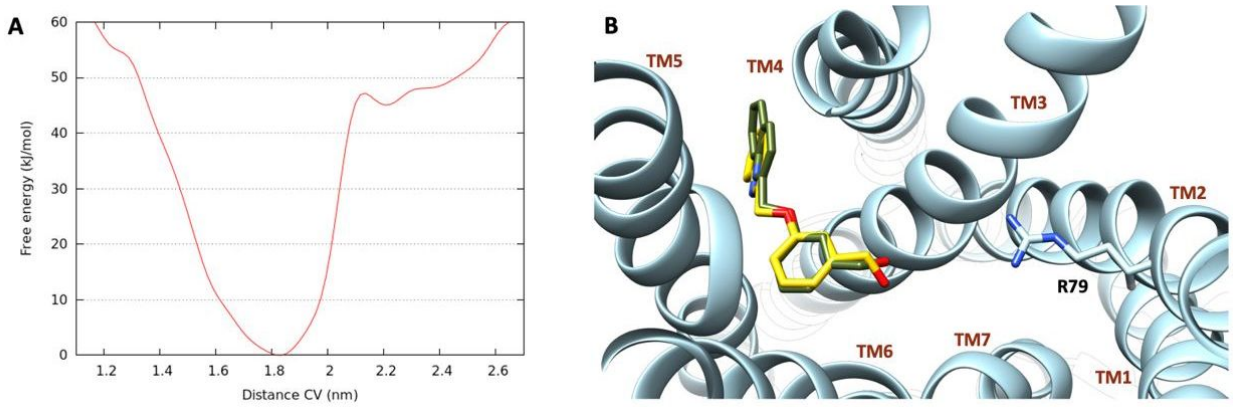

Figure 9. Results from **5** MetaD calculations. **A**) Free energy profile of **5** in $CysLT_1R$ binding pocket; **B**) Comparison between the energetically most stable binding pose obtained from MetaD (gold sticks), and the centroid of the MD most populated cluster (dark green sticks). $Arg79^{2.60}$ is shown as cyan sticks and labelled. Oxygen atoms are depicted in red and nitrogen atoms in blue. The receptor is represented as cyan ribbons with its TMs labelled. Hydrogens are omitted for the sake of clarity.

Binding mode of 6 in GPBAR1. Compound **6** is the second most potent dual ligand of the series that we decided to study in $CysLT_1R$ and GPBAR1. As regards GPBAR1, we benefited from the protein conformation obtained from the MD simulation on the **5**/GPBAR1 complex and used such structure for the following docking calculations (see Methods for details). In fact, in this receptor state, the conformation of the binding site residues is optimized to host compound **5**, which is structurally similar to **6**, thus improving the reliability of the docking calculations. In the best-scored docking pose, **6** interacts with GPBAR1 very similarly to **5** (Figure 6A). In particular, the quinoline scaffold lodges in the amphipathic cleft formed by TM3, TM5 and TM6 where it engages favorable interactions with residues $Tyr89^{3.29}$, $Leu97^{3.37}$, $Glu169^{5.43}$, $Leu173^{5.46}$, $Tyr240^{6.51}$, $Val241^{6.52}$, $Leu244^{6.55}$. As with **5**, the quinoline moiety H-bonds with $Asn93^{3.33}$ and forms π-π stacking interactions with $Phe96^{3.36}$. Furthermore, the ligand's phenyl ring engages a T-shaped π stacking interaction with $Trp237^{6.48}$ and points towards TM2 and TM7 forming apolar interactions with $Leu68^{2.57}$, $Leu71^{2.60}$, $Thr74^{2.63}$, $Pro92^{3.32}$, and $Leu266^{7.39}$. Finally, the carboxyl group establishes a H-bond with $Ser270^{7.43}$ (Figure 10A).

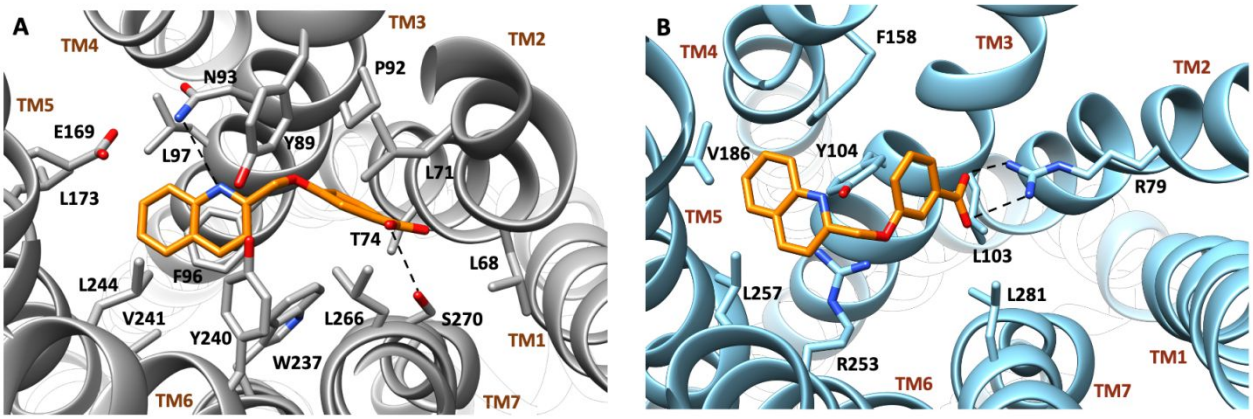

Figure 10. Binding mode of **6** in (***A***) GPBAR1 and (***B***) $CysLT_1R$. The ligand is represented as orange sticks, whereas the interacting residues of the receptors are shown in grey (GPBAR1) or cyan ($CysLT_1R$) and labelled. Oxygen atoms are depicted in red and nitrogen atoms in blue. The receptors are represented as grey (GPBAR1) or cyan ($CysLT_1R$) ribbons with their TMs labelled. Hydrogens are omitted for the sake of clarity and H-bonds and salt bridges are displayed as black dashed lines.

Binding mode of 6 in $CysLT_1R$. Following the same approach adopted for GPBAR1, docking of **6** to $CysLT_1R$ was performed using the protein conformation retrieved from the MD simulation on the **5**/$CysLT_1R$ (see Methods for details). In $CysLT_1R$, **6** occupies the binding site similarly to **5**, however, few differences arise. As seen in **5**, the quinoline ring is located close to TM4 and TM5, forming several hydrophobic contacts with residues like Phe158$^{4.60}$, Val186$^{5.35}$ and Leu257$^{6.59}$. Furthermore, **6** forms a T-shaped π and cation-π interaction with Tyr104$^{3.33}$ and Arg253$^{6.55}$, respectively. At variance with **5**, compound **6** points the phenyl group towards TM3 and TM2 contacting with Leu103$^{3.32}$ and Leu281$^{7.39}$, and above all the salt bridge interaction through its carboxyl group with Arg79$^{2.60}$ (Figure 10B).

Binding mode of 14 in GPBAR1. Finally, we investigated the binding mechanism of **14**, the most potent selective GPBAR1 ligand generated in this study. Similarly to **5** and **6**, **14** places its quinoline scaffold between TM3 and TM5 where H-bonds with Asn93$^{3.33}$ and establishes hydrophobic interactions with Leu97$^{3.37}$, Leu100$^{3.40}$, Leu173$^{5.46}$ and Leu174$^{5.47}$. The phenyl group interacts with Pro92$^{3.32}$ and makes a T-shaped π interaction with Phe96$^{3.36}$. Finally, the alkyl group

extends towards TM1 and TM7 making additional hydrophobic contacts with Leu68$^{2.57}$, Leu71$^{2.60}$ and Leu266$^{7.39}$ (Figure 11).

We finally note that the binding poses of **5**, **6** and **14** are in good agreement with the data previously reported for REV5901 (Figure S3).[11] In particular, the interactions with residues known to play an important role in the binding of REV5901 and other GPBAR1 agonists, like deoxycholic acid (DCA), are here conserved such as the H-bond with Asn93$^{3.33}$ and the hydrophobic pattern involving Tyr89$^{3.29}$, Phe96$^{3.36}$ and Trp237$^{6.48}$ (Figure S3 and S4).[11,38,40,41,42,43,53]

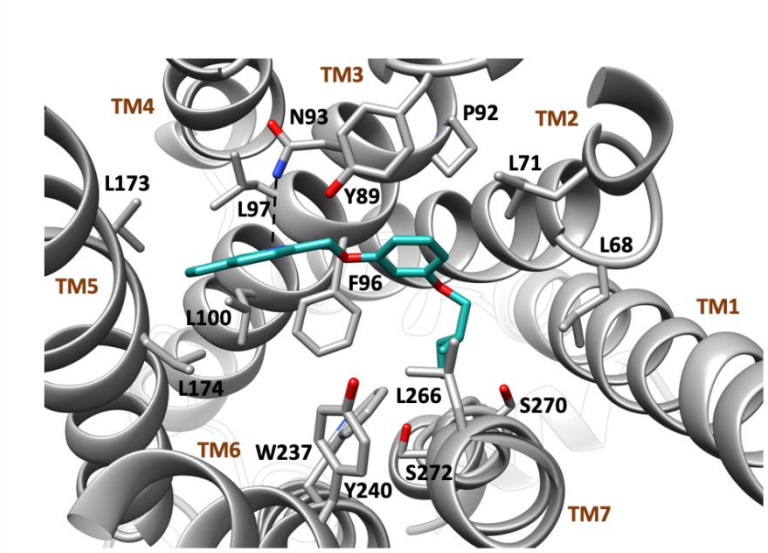

Figure 11. Binding mode of **14** in GPBAR1 from docking calculations. The ligand is represented as light sea green sticks, whereas the interacting residues of the receptor are shown in grey and labelled. Oxygen atoms are depicted in red and nitrogen atoms in blue. The receptor is represented as grey ribbons with its TMs labelled. Hydrogens are omitted for the sake of clarity and H-bonds are displayed as black dashed lines.

Pharmacokinetics evaluation. The physicochemical parameters of the above-mentioned compounds were assessed by LC-MS analysis and compared with reference compound REV5901 (Table 2). Compounds **5** and **6** are endowed with good physicochemical properties showing a better aqueous solubility than REV5901 (141 and >200, respectively, vs 39 μM). Furthermore, the liability of synthetized compounds to be modified by human metabolizing enzymes contained in liver microsomal and S9 fractions was investigated in vitro, evaluating by high-performance liquid

chromatography-MS/MS analysis the disappearance of unmodified compounds. Compounds **5** e **6** showed promising results, being highly stable to microsomal enzymes, responsible for Phase I metabolism whereas compound **14** was rapidly modified by Phase I enzymes, as reported in table 2. Therefore, the in vitro metabolic stability of compounds **5** and **6** were further investigated employing liver S9 fraction, also containing enzymes responsible for Phase II reactions. These compounds showed a very promising $t_{1/2}$ 119 and 247.5 min, respectively (CL_{int}= 19 and 9.3) and when compared with REV5901 showed less susceptibility to metabolic modifications. Indeed, REV5901 is more rapidly modified by hepatic enzymes contained in S9 fraction. All these data demonstrate the pharmacokinetic improvements of compounds **5** and **6** with respect to REV5901 and highlight their pharmacological potential in associating potency and efficacy in the dual modulation of GPBAR1/$CysLT_1R$ (Table 1) with excellent metabolic stabilities (Table 2).

Table 2. In vitro pharmacokinetics assays.

			Microsomes		S9 fraction	
Compound	Solubility (μM)[a]	LogD	$t_{1/2}$ (min)	C_{int}[b]	$t_{1/2}$ (min)	C_{int}
REV5901	39.3	3.1	37	63	57	40
5	141	2.8	48	48	119	19
6	>200	0.12	210	11	247.5	9.3
14	3.5	1.01	22.3	103.3	nd	nd

[a]Aqueous solubility at pH 7.4; [b]Reported as μL/min/mg protein. nd, not determined. Each measurement has been repeated in triplicate (three independent experiments in parallel) and SD < 5%.

Discussion and Conclusion

The present work is inspired by our recent discovery of the first dual non-steroidal ligand REV5901 as $CysLT_1R$ antagonist / GPBAR1 agonist.[11] The promising pharmacological data of REV5901 in the treatment of colitis via simultaneous modulation of $CysLT_1R$ and GPBAR1[11] prompted us to investigate the REV5901 structure in order to achieve derivatives with improved activity and

pharmacokinetic profile. In particular, we introduced on the phenoxyquinoline scaffold in different positions functional groups with diverse polarity - carboxyl, hydroxymethyl, methoxycarbonyl groups (compound **1**-**9**) - including alkylether chains of different length and flexibility - e.g., propyl, isopropyl, butyl - (compound **10**-**15**) (Figure 2). Overall, compounds **5** and **6** reveal to be the most potent dual activity compounds, while compound **14** shows the most selective profile towards GPBAR1 over $CysLT_1R$. We disclosed the structure of the binding complexes of these ligands with the two receptors and elucidated their pharmacokinetic profiles to place them in an optimal position to enter pre-clinical studies. Our results allow a solid discussion of the structure activity relationship for the new series of compounds and providing structural insights on ligand binding to $CysLT_1R$ and GPBAR1 that are helpful in guiding future drug discovery campaigns on the two targets. In particular, the effects of the different substituents on the phenoxyquinoline scaffold are different in $CysLT_1R$ and GPBAR1 and they are discussed as follows.

In the compound series **1**-**9**, the methoxycarbonyl group is less effective than the carboxyl in activating GPBAR1 in both the meta and para positions, whereas the opposite is true for $CysLT_1R$ (**1, 4** vs **3, 6**). This difference is more pronounced in the meta position for GPBAR1 and in the para one for $CysLT_1R$. Whilst the hydroxymethyl group has the same efficacy and potency for $CysLT_1R$ when attached to both the meta and para positions (**5** vs **2**), higher or similar to the methoxycarbonyl and carboxyl groups, depending on their position, (**2** vs **1, 3** and **5** vs **4, 6**), in the case of GPBAR1 the efficacy significantly increases when moving from para to meta (**5** vs **2**), to the point of reversing the efficacy of hydroxymethyl substituted compounds when compared to the carboxylic ones (**2** vs **3** and **5** vs **6**). Double functionalization of the phenoxyquinoline scaffold with a hydroxyl group in the meta position and different substitutions in the para one (**7**, **8**, **9**) led to an overall reduction of the efficacy towards $CysLT_1R$ when compared to the mono-substituted compounds. Similarly, **7** and **9** showed low efficacy towards GPBAR1, whereas good efficacy but lower potency was found for **8** when compared to **5** and **6**.

In the alkylether series (**10** to **15**), increasing the length of the alkyl chain led to a reduction of the efficacy towards $CysLT_1R$ (**13**, **14**, **15** vs **10**, **11**, **12**), whereas no significant changes were found on GPBAR1. Except for **11**, all the alkylether compounds have good efficacy towards this receptor, probably due to their similarity with REV5901. In particular, the butyl, 2-methylbutyl and the pentyl groups are selective agonists of GPBAR1 with good efficacy and high potency, better than the most potent compounds of the series **1**-**9** (**13**, **14**, **15** vs **5**, **6**). Among these, **14** has the lowest EC_{50} and good efficacy, which warranted further characterization of its properties *in-vitro*.

Furthermore, **5** and **6** showed interesting pharmacokinetic properties, while **14** suffered low aqueous solubility and chemical instability. In particular, **5** and **6** showed a very promising metabolic stability (Table 2), highlighting their pharmacological potential in associating potency and efficacy in GPBAR1/$CysLT_1R$ dual modulation with excellent pharmacokinetics.

Characterization of the binding modes of compounds **1**-**15** to GPBAR1 showed good agreement with the data previously reported.[11,40,41,42,43] In particular, in all our docking calculations the quinoline scaffold is placed between TM3, TM5 and TM6, establishing a H-bond with $Asn93^{3.33}$ which represents a hallmark of REV5901 and its derivatives binding modes.[11,38,40,41,42,43] These data were further confirmed via MD calculations performed on **5**, which showed the remarkable stability of this binding mode (Figure 8A).

In $CysLT_1R$, the binding mode of the derivatives **1**-**15** is very similar, placing the quinoline scaffold between TM3 and TM5 or TM3 and TM6, where the ligand forms a number of H-bond and aromatic interactions, typically with $Tyr104^{3.33}$, $Tyr108^{3.37}$, and $Arg253^{6.55}$. The binding mode of the quinoline series was further confirmed by the study of the most potent compound of the series, **5**, through more accurate molecular binding techniques like MD and free-energy calculations (Figure 8B, 8C and Figure 9B). Interestingly, the binding mode of **5** resembles the recently reported crystallographic binding pose of pranlukast in $CysLT_1R$ (Figure 7).[20] In fact, the occupancy of the binding site of **5** and pranlukast is similar and the hydroxyl group of **5** mimics the tetrazole moiety of pranlukast forming water-mediated H-bonds with $Arg79^{2.60}$ (Figure 6B and Figure 7). The

comparison is even more striking in the case of compound **6** where the carboxyl group establishes a salt bridge and H-bonds with Arg79$^{2.60}$, and an additional H-bond with Thr100$^{3.29}$, similarly to the tetrazole group of pranlukast (Figure 10B and Figure S2).

Taken together, our findings reveal that the presence of a polar or a negatively charged group opportunely spaced from an aromatic ring in the ligand represents a structural requirement to interact with Arg79$^{2.60}$ of $CysLT_1R$ and achieve dual $CysLT_1R$/GPBAR1 activity. On the other hand, replacing the polar group with a hydrophobic alkyl chain allows achieving selective activity on GPBAR1 over $CysLT_1R$.

From a pharmacological point view, the series of dual GPBAR1 agonists and $CysLT_1R$ antagonists described herein, present several important features. Indeed, we have shown that three best compounds of this series - i.e. compound **5, 6** and **14** - perform a series of pharmacological effects that can be ascribed to their dual activity as GPBAR1 agonists and $CysLT_1R$ antagonists (i.e. **5** and **6**) or to their selective activity on GPBAR1 as for **14**. Using in vitro models, we have shown that **5** and **6** are efficacious in antagonizing effects promoted by activation of $CysLT_1R$, while the anti-inflammatory activity exerted by their GPBAR1 agonism is fully maintained. Accordingly with the activity toward GPBAR1, all three agents blunted the generation of inflammatory cytokines induced by exposure of murine macrophages to LPS and reversed the endothelial cells/monocytes adhesion. Because adhesion of monocytic cells to the endothelial cells is the first step involved in the emigration of leukocytes into inflamed tissues, the beneficial effects observed with the three ligands is of interest and might be useful in reducing inflammation in various inflammatory settings. The fact that the novel chemical entities hit two different receptors, make them interesting pharmacological candidates in a broad range of diseases, including colitis and gastrointestinal inflammatory disorders,[54,55,56] although further pharmacological characterization is needed.

In conclusion, compounds endowed with dual activity in the micromolar range, like REV5901, represent a valid starting point to identify novel ligands with improved structural properties and activity. To this end, simplifying the chemical structure of the dual-active compound, however

maintaining its potency towards the two GPCRs, is a fundamental step in the drug design strategy. This is what we achieved in this work by removing at the same time the secondary hydroxyl group and the asymmetric center and reducing the size of REV5901, leading to the discovery of two equally potent dual ligands, compounds **5** and **6**, and a selective GPBAR1 agonist, compound **14**. The obtained compounds have better synthetic accessibility and present the minimal structural requisites - functional groups - to achieve activity towards $CysLT_1R$ and GPBAR1, thus representing a precious starting point for lead optimization studies. In the proposed new series of quinoline derivatives, our findings show that the *meta*-substituted derivatives, compounds **5** and **6**, are the most effective dual activity ligands so far identified, with promising pharmacokinetic properties and therapeutic potential in the treatment of colitis, metabolic syndromes and other GPBAR1/$CysLT_1R$ related diseases. Furthermore, we present here the first structure-based rationalization of ligand binding to $CysLT_1R$, achieved through the combined application of experimental and *in-silico* techniques, which will ultimately help in guiding future drug discovery studies on $CysLT_1R$ and GPBAR1.

Experimental Section

Chemistry. High-resolution ESI-MS spectra were performed with a LTQ-XL equipped with an Ultimate 3000 HPLC system (Thermo Fisher scientific) mass spectrometer. NMR spectra were obtained on Bruker 400 spectrometer (^1H at 400, ^{13}C at 100 MHz), recorded in $CDCl_3$ (δ_H =7.26 and δ_C =77.0 ppm) and CD_3OD (δ_H=3.30 and δ_C=49.0 ppm). *J* are in hertz and chemical shifts (δ) are reported in ppm and referred to $CHCl_3$ and CHD_2OD as internal standards. HPLC was performed using a Waters Model 510 pump equipped with Waters Rheodine injector and a differential refractometer, model 401 and processed with Clarity™ chromatography software. Reaction progress was monitored via thin-layer chromatography (TLC) on Alugram® silica gel G/UV254 plates. Silica gel MN Kieselgel 60 (70-230 mesh) from Macherey-Nagel Company was

used for column chromatography. The chemicals were obtained from Zentek or Sigma Aldrich. Tetrahydrofuran, diethyl ether and triethylamine were distilled from calcium hydride immediately prior to use. All reactions were carried out under argon atmosphere using flame-dried glassware. The purity of all the intermediates, checked by ^{1}H NMR, was greater than 95%. The purity of tested compounds was determined to be always greater than 95% by analytical HPLC analysis as reported for each compound**.**

General procedures.

DIBAL-H reduction. At a solution of methyl quinoline-2-carboxylate in dry THF (25 mL) at 0 °C, a solution of DIBAL-H (2.0 eq, 1.0 M in THF) was added dropwise. The resulting mixture was stirred at room temperature for 8h at 0 °C. When the TLC shows the end of the substrate, the reaction was quenched by slow addition of a solution of saturated sodium potassium tartrate and, after dilution with CH_2Cl_2, stirred for 2h. The mixture was partitioned three times with CH_2Cl_2, and the combined organic extracts dried over Na_2SO_4. The solution was concentrated in vacuum and the residue was further purified on silica column using 6:4 v/v hexane/ethyl acetate and 0.1% TFA, to give **17** in quantitative yield.

Mitsunobu reaction. At a solution of PPh_3 (3.5 eq) in dry THF a 0 °C, 3.5 eq of diisopropyl azodicarboxylate (DIAD) were added dropwise. After 10 minutes, a solution of alcohol **17** in dry THF was added and the mixture was stirred for further 10 minutes before adding a solution of methyl 4-hydroxybenzoate or methyl 3-hydroxybenzoate in dry THF. The mixture was stirred vigorously for 12h, then partitioned between water and EtOAc (3 x 50 mL). The organic layer was collected and washed twice with aqueous KOH 2.5 M solution, then with brine, dried over Na_2SO_4, filtered, and concentrated under reduced pressure. The resulted residue was purified on silica column to give compounds **1** and **4**, respectively.

Methyl 4-(quinolin-2-ylmethoxy)benzoate (1). Purification by flash column chromatography (silica gel, hexane: ethyl acetate 8:2 and 0.1% of TEA) furnished compound **1** (76% yield). An analytic sample was further purified by HPLC on a Nucleodur 100-5 C18 column (5 μm; 10 mm

i.d. x 250 mm) with MeOH/H_2O 82:18 v/v as eluent (flow rate 3 mL/min, t_R = 13 min); ^{1}H NMR ($CDCl_3$, 400 MHz): δ 8.21 (1H, d, *J* = 8.5 Hz), 8.09 (1H, d, *J* = 8.3 Hz), 8.00 (2H, d, *J* = 9.0 Hz), 7.84 (1H, d, *J* = 8.3 Hz), 7.76 (1H, t, *J* = 8.3 Hz), 7.65 (1H, d, *J* = 8.5 Hz), 7.57 (1H, t, *J* = 8.3 Hz), 7.06 (2H, d, *J* = 9.0 Hz), 5.43 (2H, s), 3.88 (3H, s). ^{13}C NMR ($CDCl_3$, 100 MHz) δ 166.7, 162.0, 157.1, 147.4, 137.1, 131.5 (2C), 129.9, 128.9, 127.7, 127.6, 126.6, 123.0, 118.9, 114.6 (2C), 71.3, 51.7. HRMS-ESI *m/z* 294.1128 [M+H$^+$], $C_{18}H_{16}NO_3$ requires 294.1125.

Methyl 3-(quinolin-2-ylmethoxy)benzoate (4). Chromatographic purification of the residue (silica gel, hexane: ethyl acetate 9:1 v/v and 0.1% of TEA) gave compound **4** (78% yield). An analytic sample was further purified by HPLC on a Nucleodur 100-5 C18 column (5 μm; 10 mm i.d. x 250 mm) with MeOH/H_2O 82:18 v/v as eluent (flow rate 3 mL/min, t_R = 14.8 min); ^{1}H NMR ($CDCl_3$, 400 MHz): δ 8.22 (1H, d, *J* = 8.4 Hz), 8.10 (1H, d, *J* = 8.0 Hz), 7.85 (1H, d, *J* = 8.0 Hz), 7.74 (2H, ovl), 7.68 (2H, ovl), 7.57 (1H, t, *J* = 8.0 Hz), 7.37 (1H, t, *J* = 7.7 Hz), 7.24 (1H, d, *J* = 7.7 Hz), 5.44 (2H, s), 3.91 (3H, s). ^{13}C NMR ($CDCl_3$, 100 MHz) δ 169.6, 158.4, 157.3, 147.5, 137.1, 131.6, 129.8, 129.5, 128.9, 127.7, 127.6, 126.6, 122.4, 119.7, 119.0, 115.6, 71.4, 52.1. HRMS-ESI *m/z* 294.1127 [M+H$^+$], $C_{18}H_{16}NO_3$ requires 294.1125.

Synthesis of (4-(quinolin-2-ylmethoxy)phenyl)methanol (2) and (3-(quinolin-2-ylmethoxy)phenyl)methanol (5). DIBAL-H reduction on esters **1** and **4** in the same experimental conditions previously reported for methyl quinoline-2-carboxylate, gave compounds **2** and **5**, respectively.

(4-(Quinolin-2-ylmethoxy)phenyl)methanol (2). Chromatographic purification on the residue (silica gel, CH_2Cl_2: MeOH 99:1 v/v) gave compound **2** (68% yield). An analytic sample was further purified by HPLC on a Nucleodur 100-5 C18 column (5 μm; 10 mm i.d. x 250 mm) with MeOH/H_2O 40:60 v/v as eluent (flow rate 3 mL/min, t_R = 15.8 min); ^{1}H NMR ($CDCl_3$, 400 MHz): δ 8.21 (1H, d, *J* = 8.0 Hz), 8.12 (1H, d, *J* = 7.3 Hz), 7.84 (1H, d, *J* = 7.3 Hz), 7.76 (1H, t, *J* = 7.3 Hz), 7.68 (1H, d, *J* = 8.0 Hz), 7.57 (1H, t, *J* = 7.3 Hz), 7.30 (2H, d, *J* = 8.0 Hz), 7.02 (2H, d, *J* = 8.0 Hz), 5.41 (2H, s), 4.62 (2H, s). ^{13}C NMR ($CDCl_3$, 100 MHz) δ 157.9, 157.8, 147.4, 137.1, 133.8,

129.8, 128.8, 128.7 (2C), 127.6, 127.5, 126.5, 119.0, 114.9 (2C), 71.1, 64.7. HRMS-ESI *m/z* 266.1178 [M+H$^+$], $C_{17}H_{16}NO_2$ requires 266.1176.

(3-(Quinolin-2-ylmethoxy)phenyl)methanol (5). Purification by flash column chromatography (silica gel, CH_2Cl_2: MeOH 99:1 v/v) furnished compound **5** (60% yield). An analytic sample was further purified by HPLC on a Nucleodur 100-5 C18 column (5 μm; 10 mm i.d. x 250 mm) with MeOH/H_2O 75:15 v/v as eluent (flow rate 3 mL/min, t_R = 11 min); ^{1}H NMR ($CDCl_3$, 400 MHz): δ 8.20 (1H, d, *J* = 8.4 Hz), 8.10 (1H, d, *J* = 7.4 Hz), 7.84 (1H, d, *J* = 7.4 Hz), 7.75 (1H, t, *J* = 7.4 Hz), 7.68 (1H, d, *J* = 8.4 Hz), 7.56 (1H, t, *J* = 7.4 Hz), 7.28 (1H, dd, *J* = 7.3, 8.0 Hz), 7.08 (1H, s), 7.0 (1H, d, *J* = 8.4 Hz), 6.95 (1H, d, *J* = 7.3 Hz), 5.40 (2H, s), 4.68 (2H, s). ^{13}C NMR ($CDCl_3$, 100 MHz) δ 158.6, 157.8, 147.4, 142.8, 137.1, 129.8, 129.6, 128.7, 127.7, 127.6, 126.5, 119.6, 119.1, 113.9, 113.4, 71.1, 64.9. HRMS-ESI *m/z* 266.1179 [M+H$^+$], $C_{17}H_{16}NO_2$ requires 266.1176.

Basic hydrolysis. An aliquot of esters **1** and **4** was dissolved in MeOH/H_2O (1:1 v/v) and treated with NaOH (5 mol eq.) at 0 °C. The resulting mixture was stirred under reflux for 8 h. The mixture was treated with 6N HCl, until pH reached 7-8, then was partitioned three times with ethyl acetate and the combined organic extracts were dried over Na_2SO_4. The solution was concentrated in vacuum. The residue was purified on silica column to give carboxylic acids **3** and **6**, respectively.

4-(Quinolin-2-ylmethoxy)benzoic acid (3). Purification by flash column chromatography (silica gel, CH_2Cl_2: MeOH 99:1) furnished compound **3** (43% yield). An analytic sample was further purified by HPLC on a Phenomenex Luna C18 column (5 μm; 4.6 mm i.d. x 250 mm), with MeOH/H_2O 60:40 v/v and 0.1% of TFA as eluent (flow rate 1 mL/min, t_R = 7.2 min); ^{1}H NMR (CD_3OD, 400 MHz): δ 8.62 (1H, d, *J* = 8.5 Hz), 8.15 (1H, d, *J* = 8.0 Hz), 8.07 (1H, d, *J* = 8.0 Hz), 8.02 (2H, d, *J* = 8.6 Hz), 7.92 (1H, t, *J* = 8.0 Hz), 7.86 (1H, d, *J* = 8.5), 7.73 (1H, t, *J* = 8.0), 7.17 (2H, d, *J* = 8.6 Hz), 5.53 (2H, s). ^{13}C NMR (CD_3OD, 100 MHz) δ 169.4, 163.4, 158.1, 147.0, 140.6, 132.8 (2C), 132.3, 129.3 (2C), 128.6, 127.9, 124.9, 120.8, 115.6 (2C), 71.1. HRMS-ESI *m/z* 278.0825 [M-H$^-$], $C_{17}H_{12}NO_3$ requires 278.0823.

3-(Quinolin-2-ylmethoxy)benzoic acid (6). Purification of compound **6** (68% yield) was carried out on column chromatography by silica gel, using CH_2Cl_2: MeOH 99:1 v/v as eluent. An analytic sample was purified by HPLC on a Nucleodur 100-5 column (5 μm; 10 mm i.d. x 250 mm), with hexane/ ethyl acetate 40:60 v/v (flow rate 3 mL/min, t_R = 6.9 min).

^{1}H NMR (CD_3OD, 400 MHz): δ 8.40 (1H, d, *J* = 8.5 Hz), 8.06 (1H, d, *J* = 8.3 Hz), 7.95 (1H, d, *J* = 8.3 Hz), 7.80 (1H, t, *J* = 8.3 Hz), 7.74 (1H, d, *J* = 8.5 Hz), 7.70 (1H, s), 7.64 (1H, t, *J* = 8.3 Hz), 7.62 (1H, d ovl), 7.41 (1H, t), 7.30 (1H, dd, *J* = 1.5, 8.0 Hz), 5.42 (2H, s); ^{13}C NMR (CD_3OD, 100 MHz) δ 169.4, 159.9, 158.8, 148.4, 139.1, 133.5, 131.3, 130.7, 129.2, 129.1, 129.0, 128.0, 123.7, 120.8, 120.7, 116.6, 71.9. HRMS-ESI *m/z* 278.0827 [M-H$^-$], $C_{17}H_{12}NO_3$ requires 278.0823.

Synthetic procedures to prepare compounds 7-9.

TBS protection. Synthesis of Compound 19**.** To a solution of the methyl 3,5-dihydroxybenzoate (2.0 g, 12 mmol), imidazole (1.5 eq), and dry DMF (10 mL) was added portion wise TBSCl (1.2 eq). The reaction mixture was stirred at RT for 1 h. The mixture was concentrated *in vacuo*, diluted with NH_4Cl saturated solution, and extracted with diethyl ether (3x50 mL). The combined organics were washed with brine, dried, and concentrated to provide the product as an oil which was purified on silica gel, using CH_2Cl_2: MeOH 95:5 as eluent (50 % yield).

Compound 20. To a solution of **17** (1.6 g, 10 mmol) in dry diethyl ether (10 mL) at -20°C was added dry TEA (6.0 eq) followed by $MeSO_2Cl$ (5.0 eq). The reaction mixture was stirred at -20° C for 30 min and then allowed to warm to RT over 2 h. The mixture was quenched with aqueous saturated solution of $NaHCO_3$ (10 mL) and extracted with diethyl ether (3 x 30 mL). The combined organics were washed with H_2O (20 mL), brine (20 mL), dried (Na_2SO_4), and concentrated under vacuum to give crude **20** in quantitative yield.

Williamson reaction. The crude mesylate **20** (1.2 eq) was added to a stirred mixture of **19** (1.0 eq), K_2CO_3 (2.5 eq), and dry DMF. The reaction mixture was stirred at 100° C for 12 h and then diluted with H_2O and extracted with ethyl acetate (3 x 30 mL). The combined organics were washed with

brine, dried (Na_2SO_4), concentrated, and purified by flash chromatography (hexane/ ethyl acetate 95:5 v/v) to provide compound **21** (87% yield).

TBS cleavage. A mixture of the compound **21** and TBAF (5.0 eq) in dry THF (3 mL) was stirred at RT overnight. Upon completion, the resulting solution was concentrated to give **7**.

Methyl 3-hydroxy-5-(quinolin-2-ylmethoxy)benzoate (7). Purification by flash column chromatography (silica gel, CH_2Cl_2: MeOH 998:2 v/v) furnished compound **7** (85% yield). An analytic sample was further purified by HPLC on a Nucleodur 100-5 column (5 μm; 10 mm i.d. x 250 mm) with hexane/ethyl acetate 7:3 v/v as eluent (flow rate 3 mL/min, t_R = 23.7 min); ^{1}H NMR (400 MHz, $CDCl_3$): δ 8.17 (1H, d, *J* = 8.5 Hz), 8.00 (1H, d, *J* = 8.0 Hz), 7.79 (1H, d, *J* = 8.0 Hz), 7.68 (1H, t, *J* = 8.0 Hz), 7.62 (1H, t, *J* = 8.5 Hz), 7.54 (1H, t, *J* = 8.0 Hz), 7.28 (1H, s), 7.21 (1H, s), 6.76 (1H, s), 5.38 (2H, s), 3.89 (3H, s). ^{13}C NMR (100 MHz, $CDCl_3$): δ 167.2, 159.1, 157.9, 157.3, 146.7, 137.8, 131.8, 130.2, 127.8, 127.7, 127.6, 126.8, 119.2, 109.8, 107.8, 106.8, 70.4, 52.1. HRMS-ESI *m/z* 310.1077 [M+H$^+$], $C_{18}H_{16}NO_4$ requires 310.1074.

3-(Hydroxymethyl)-5-(quinolin-2-ylmethoxy)phenol (8) and 3-hydroxy-5-(quinolin-2-ylmethoxy)benzoic acid (9). DIBAL-H reduction and NaOH hydrolysis on **7**, in the same experimental conditions previously reported for methyl quinoline-2-carboxylate, gave compounds **8** and **9**, respectively.

3-(Hydroxymethyl)-5-(quinolin-2-ylmethoxy)phenol (8). Purification of **8** (92% yield) was carried out on silica gel, using CH_2Cl_2: MeOH 95:5 v/v as eluent. An analytic sample was purified by HPLC on a PFP C18 column (5 μm; 4.6 mm i.d. x 250 mm), with MeOH/H_2O 60:40 v/v and 0.1% TFA (flow rate 1 mL/min, t_R = 12.2 min). ^{1}H NMR (400 MHz, $CDCl_3$): δ 8.20 (1H, d, *J* = 8.5 Hz), 8.10 (1H, d, *J* = 8.0 Hz), 7.84 (1H, d, *J* = 8.0 Hz), 7.75 (1H, t, *J* = 8.0 Hz), 7.67 (1H, d, *J* = 8.5 Hz), 7.57 (1H, t, *J* = 8.0 Hz), 6.65 (1H, s), 6.49 (1H, s), 6.46 (1H, s), 5.40 (2H, s), 4.62 (2H, s). ^{13}C NMR (100 MHz, $CDCl_3$): δ 161.1, 159.8, 159.6, 148.3, 145.5, 139.0, 131.3, 129.1, 129.0, 128.9, 127.9, 120.6, 107.8, 105.5, 102.1, 71.6, 65.1. HRMS-ESI *m/z* 282.1127 [M+H$^+$], $C_{17}H_{16}NO_3$ requires 282.1125.

3-Hydroxy-5-(quinolin-2-ylmethoxy)benzoic acid (9). Purification of compound **9** (quantitative yield) was carried out in column chromatography by silica gel, using DCM: MeOH 95:5 v/v as eluent. An analytic sample was purified by HPLC on a PFP C18 (5 μm; 4.6 mm i.d. x 250 mm), with MeOH/H_2O 55:45 v/v and 0.1% TFA (flow rate 1 mL/min, t_R = 9.2 min). ^{1}H NMR (400 MHz, CD_3OD): δ 8.39 (1H, d, *J* = 8.4 Hz), 8.05 (1H, d, *J* = 8.0 Hz), 7.96 (1H, d, *J* = 8.0 Hz), 7.79 (1H, t, *J* = 8.0 Hz), 7.72 (1H, d, *J* = 8.4 Hz), 7.62 (1H, t, *J* = 8.0 Hz), 7.18 (1H, s), 7.08 (1H, s), 6.66 (1H, s), 5.37 (2H, s). ^{13}C NMR (100 MHz, CD_3OD): δ 160.7, 159.7, 158.2, 148.2, 139.1, 131.4, 131.3, 129.2, 129.1, 129.0, 128.9, 128.0, 120.6, 110.8, 107.8, 107.0, 71.8. HRMS-ESI *m/z* 294.0775 [M-H$^-$], $C_{17}H_{12}NO_4$ requires 294.0772.

Synthetic procedures to prepare alkylaril-ethers 10-15.

TBS protection on resorcinol (**22**) (47%) followed by Mitsunobu reaction with several different alcohols (propan-1-ol, propan-2-ol, butan-2-ol, butan-1-ol, 2-methylbutan-1-ol, and pentan-1-ol) and TBS cleavage in the same experimental conditions previously described furnished compounds **24-29** in 47-84% yields.

Finally, Williamson ether synthesis between **24-29** and quinolin-2-yl methyl methane sulfonate (**20**) with the same experimental procedures previously described gave compounds **10-15**.

2-((3-propoxyphenoxy)methyl)quinoline (10). HPLC purification on a Nucleodur 100-5 column (5 μm; 10 mm i.d. x 250 mm) eluting with hexane/ethyl acetate 9:1 v/v (flow rate 3 mL/min, t_R = 16.5 min) gave compound **10** in quantitative yield. ^{1}H NMR (400 MHz, $CDCl_3$): δ 8.20 (1H, d, *J* = 8.6 Hz), 8.09 (1H, d, *J* = 7.5 Hz), 7.84 (1H, d, *J* = 7.5 Hz), 7.74 (1H, t, *J* = 7.5 Hz), 7.68 (1H, d, *J* = 8.6 Hz), 7.56 (1H, t, *J* = 7.5 Hz), 7.17 (1H, t, *J* = 8.0 Hz), 6.63 (1H, s), 6.61 (1H, ovl), 6.54 (1H, dd, *J* = 8.0, 2.0 Hz), 5.38 (2H, s), 3.90 (2H, t, *J* = 7.0 Hz), 1.80 (2H, sextet, *J* = 7.0 Hz), 1.03 (3H, t, *J* = 7.0 Hz). ^{13}C NMR (100 MHz, $CDCl_3$): δ 160.4, 159.7, 157.9, 147.6, 137.0, 130.0, 129.7, 129.0, 127.7, 127.6, 126.5, 119.2, 107.6, 106.8, 101.8, 71.1, 69.7, 22.5, 10.5. HRMS-ESI *m/z* 294.1492 [M+H$^+$], $C_{19}H_{20}NO_2$ requires 294.1489.

2-((3-isopropoxyphenoxy)methyl)quinoline (11). HPLC purification on a Nucleodur 100-5 column (5 μm; 10 mm i.d. x 250 mm), eluting with hexane/ethyl acetate 95:5 v/v (flow rate 3 mL/min, t_R = 38 min) gave compound **11** in 61% yield. ^{1}H NMR (400 MHz, $CDCl_3$): δ 8.19 (1H, d, *J* = 8.6 Hz), 8.09 (1H, d, *J* = 7.5 Hz), 7.84 (1H, d, *J* = 7.5 Hz), 7.74 (1H, t, *J* = 7.5 Hz), 7.68 (1H, d, *J* = 8.6 Hz), 7.56 (1H, t, *J* = 7.5 Hz), 7.17 (1H, t, *J* = 8.0 Hz), 6.61 (1H, s), 6.60 (1H, ovl), 6.52 (1H, dd, *J* = 8.0, 2.0 Hz),5.38 (2H, s), 4.52 (1H, septet, *J* = 6.0 Hz), 1.32 (6H, d, *J* = 6.0 Hz). ^{13}C NMR (100 MHz, $CDCl_3$): δ 159.6, 159.2, 157.9, 147.5, 136.9, 129.9, 129.7, 128.9, 127.7, 127.6, 126.4, 119.1, 108.8, 106.8, 103.0, 71.3, 69.9, 22.0 (2C). HRMS-ESI *m/z* 294.1493 [M+H$^+$], $C_{19}H_{20}NO_2$ requires 294.1489.

2-((3-(sec-butoxy)phenoxy)methyl)quinoline (12). HPLC purification on a Nucleodur 100-5 column (5 μm; 10 mm i.d. x 250 mm) eluting with hexane/ethyl acetate 9:1 v/v (flow rate 3 mL/min, t_R = 15 min) gave compound **12** in quantitative yield. ^{1}H NMR (400 MHz, $CDCl_3$): δ 8.19 (1H, d, *J* = 8.6 Hz), 8.09 (1H, d, *J* = 7.5 Hz), 7.84 (1H, d, *J* = 7.5 Hz), 7.74 (1H, t, *J* = 7.5 Hz), 7.68 (1H, d, *J* = 8.6 Hz), 7.56 (1H, t, *J* = 7.5 Hz), 7.17 (1H, t, *J* = 8.0 Hz), 6.61 (1H, s), 6.60 (1H, ovl), 6.52 (1H, dd, *J* = 8.0, 2.0 Hz), 5.37 (2H, s), 4.27 (2H, sextet, *J* = 6.1 Hz), 1.73 (1H, m), 1.60 (1H, m), 1.27 (2H, d, *J* = 6.1 Hz), 0.96 (3H, t, *J* = 7.4 Hz). ^{13}C NMR (100 MHz, $CDCl_3$): δ 159.7, 159.6, 158.0, 147.5, 136.9, 129.9, 129.7, 128.9, 127.7, 127.6, 126.4, 119.2, 108.9, 106.7, 103.1, 75.2, 71.1, 29.2, 19.2, 9.9. HRMS-ESI *m/z* 308.1647 [M+H$^+$], $C_{20}H_{22}NO_2$ requires 308.1645.

2-((3-butoxyphenoxy)methyl)quinoline (13). HPLC purification on a Nucleodur 100-5 column (5 μm; 10 mm i.d. x 250 mm) eluting with hexane/ethyl acetate 9:1 v/v (flow rate 3 mL/min, t_R = 17.3 min) gave compound **13** in quantitative yield. ^{1}H NMR (400 MHz, $CDCl_3$): δ 8.19 (1H, d, *J* = 8.6 Hz), 8.09 (1H, d, *J* = 7.5 Hz), 7.84 (1H, d, *J* = 7.5 Hz), 7.74 (1H, t, *J* = 7.5 Hz), 7.68 (1H, d, *J* = 8.6 Hz), 7.56 (1H, t, *J* = 7.5 Hz), 7.17 (1H, t, *J* = 8.0 Hz), 6.61 (1H, s), 6.60 (1H, ovl), 6.52 (1H, dd, *J* = 8.0, 2.0 Hz), 5.38 (2H, s), 3.95 (2H, t, *J* = 7.0 Hz), 1.75 (2H, pentet, *J* = 7.0 Hz), 1.48 (2H, sextet, *J* = 7.4 Hz), 0.97 (3H, t, *J* = 7.4 Hz). ^{13}C NMR (100 MHz, $CDCl_3$): δ 160.5, 159.6, 158.0, 147.6,

137.0, 129.9, 129.7, 128.9, 127.7, 127.6, 126.5, 119.1, 107.6, 106.8, 101.7, 71.2, 67.7, 31.3, 19.2, 13.8. HRMS-ESI *m/z* 308.1648 [M+H$^+$], $C_{20}H_{22}NO_2$ requires 308.1645.

2-((3-(2-methylbutoxy)phenoxy)methyl)quinoline (14). HPLC purification on a Nucleodur 100-5 column (5 μm; 10 mm i.d. x 250 mm) eluting with hexane/ethyl acetate 9:1 v/v (flow rate 3 mL/min, t_R = 14.0 min) gave compound **14** in 90%. ^{1}H NMR (400 MHz, $CDCl_3$): δ 8.19 (1H, d, *J* = 8.6 Hz), 8.09 (1H, d, *J* = 7.5 Hz), 7.84 (1H, d, *J* = 7.5 Hz), 7.74 (1H, t, *J* = 7.5 Hz), 7.68 (1H, d, *J* = 8.6 Hz), 7.56 (1H, t, *J* = 7.5 Hz), 7.17 (1H, t, *J* = 8.0 Hz), 6.61 (1H, s), 6.60 (1H, ovl), 6.52 (1H, dd, *J* = 8.0, 2.0 Hz), 5.38 (2H, s), 3.80 (1H, dd, *J* = 9.0, 6.0 Hz), 3.71 (1H, dd, *J* = 9.0, 6.6 Hz), 1.85 (1H, septet, J = 6.6 Hz), 1.56 (1H, m), 1.25 (1H, m), 1.00 (3H, d, *J* = 6.6 Hz), 0.94 (3H, t, *J* = 7.3 Hz). ^{13}C NMR (100 MHz, $CDCl_3$): δ 160.6, 159.6, 158.0, 147.5, 136.9, 129.9, 129.8, 128.9, 127.8, 127.6, 126.5, 119.1, 107.7, 106.8, 101.8, 73.0, 71.2, 34.6, 26.1, 16.5, 11.3. HRMS-ESI *m/z* 322.1805 [M+H$^+$], $C_{21}H_{24}NO_2$ requires 322.1802.

2-((3-(pentyloxy)phenoxy)methyl)quinoline (15). HPLC purification on a Nucleodur 100-5 column (5 μm; 10 mm i.d. x 250 mm) eluting with hexane/ethyl acetate 9:1 v/v (flow rate 3 mL/min, t_R = 13.8 min) gave compound **15** in 95% yield. ^{1}H NMR (400 MHz, $CDCl_3$): δ 8.19 (1H, d, *J* = 8.6 Hz), 8.09 (1H, d, *J* = 7.5 Hz), 7.84 (1H, d, *J* = 7.5 Hz), 7.74 (1H, t, *J* = 7.5 Hz), 7.68 (1H, d, *J* = 8.6 Hz), 7.56 (1H, t, *J* = 7.5 Hz), 7.17 (1H, t, *J* = 8.0 Hz), 6.61 (1H, s), 6.60 (1H, ovl), 6.52 (1H, dd, *J* = 8.0, 2.0 Hz), 5.38 (2H, s), 3.93 (2H, t, *J* = 7.0 Hz), 1.77 (2H, m), 1.40 (4H, m), 0.93 (3H, t, *J* = 7.0 Hz). ^{13}C NMR (100 MHz, $CDCl_3$): δ 160.4, 159.6, 157.9, 147.5, 136.9, 129.9, 129.7, 128.9, 127.7, 127.6, 126.4, 119.1, 107.6, 106.8, 101.8, 71.2, 68.0, 28.9, 28.2, 22.4, 13.9. HRMS-ESI *m/z* 322.1807 [M+H$^+$], $C_{21}H_{24}NO_2$ requires 322.1802.

In vitro assay.

Transactivation assay. To evaluate GPBAR1 mediated transactivation, HEK-293T cells were transfected with 200 ng of human pGL4.29 (Promega), a reporter vector containing a cAMP response element (CRE) that drives the transcription of the luciferase reporter gene luc2P, with 100 ng of pCMVSPORT6-human GPBAR1, and with 100 ng of pGL4.70. At 24 h post-transfection,

cells were stimulated 18 h with 10 μM TLCA and compounds **1-15.** After treatments, cells were lysed in 100 μL of lysis buffer (25 mM Tris-phosphate, pH 7.8; 2 mM DTT; 10% glycerol; 1% Triton X-100), and 10 μL of cellular lysate was assayed for luciferase activity using the luciferase assay system (Promega). Luminescence was measured using Glomax 20/20 luminometer (Promega). Luciferase activities were assayed and normalized with Renilla activities.

Human $CysLT_1$ (LTD4) (h) (antagonist effect) Cellular Functional Assay. These assays were performed at Eurofins Cerep-Panlabs (France).[23] The cells are suspended in DMEM buffer (Invitrogen), then distributed in microplates at a density of 3.104 cells/well. The fluorescent probe (Fluo4 Direct, Invitrogen) mixed with probenicid in HBSS buffer (Invitrogen) complemented with 20 mM Hepes (Invitrogen) (pH 7.4) is then added into each well and equilibrated with the cells for 60 min at 37 °C then 15 min at 22 °C. Thereafter, the assay plates are positioned in a microplate reader (CellLux, PerkinElmer) which is used for the addition of the test compound or HBSS buffer then 5 min later 0.1 nM LTD4 or HBSS buffer (basal control), and the measurements of changes in fluorescence intensity which varies proportionally to the free cytosolic Ca^{2+} ion concentration. The results are expressed as a percent inhibition of the control response to 0.1 nM LTD4. The standard reference antagonist is MK 571.

Concentration-Response Curve. For compounds showing efficacy higher than 25% on GPBAR1 we calculated the EC_{50}. The concentration response curves were performed in HEK-293T cells transfected as described above and then treated with increasing concentrations of compounds **4-6**, **8-10** and **13-15** (from 0.1 to 50 μM). At 18 h post stimulations, cellular lysates were assayed for luciferase and Renilla activities using the Dual-Luciferase Reporter assay system (E1980, Promega). Luminescence was measured using Glomax 20/20 luminometer (Promega). Luciferase activities were normalized with Renilla activities. For compounds showing efficacy higher than 60% on $CysLT_1R$ we calculated the IC_{50}. The concentration response curves were performed at Eurofins Cerep-Panlabs (France).

Cell culture. RAW264.7 cells were grown at 37 °C in D-MEM containing 10% FBS, 1% L-glutamine and 1% penicillin/streptomycin. HAEC (Human Aortic Endothelilal Cells) were cultured in endothelial cell medium (Innoprot) supplemented with 5% FBS, endothelial cell growth supplement (Innoprot) and antibiotics. U937 cell line were cultured in RPMI 1640 supplemented with 10% FBS, 1% glutamine, and 1% penicillin/streptomycin. All cells were regularly passaged to maintain exponential growth. For the first experimental set the RAW264.7 cells were classically activated with LPS (100 nM, L2880; Sigma-Aldrich, St. Louis, MO), and exposed or not to **5**, **6** and **14** at the concentration of 0.1, 1.5 and 10 μM for 16 h. After 16 h, the cells were recovered and mRNA extraction was performed to investigate gene expression. For the cell proliferation assay, RAW264.7 (25.000/well) were plated on a 24-well plate (1 mL/well) and stimulated with LTD4 (1 μM) for 48 h alone or in combination with compounds **5**, **6**, **14** and REV5901 at concentration of 10 μM. Cell counting was performed using Trypan Blu staining. For cell proliferation, MTS assay (Promega, Madison WI) was performed in parallel with the same culture and treatments conditions following instructions provided by the manufacturer.

For cell adhesion assay, HAEC cells (50 × 104) were plated on a 24-well plate (1 mL/well) and activated with TNFα (100 ng/mL) and LTD4 (1 μM) for 24 h alone or in combination with compounds at 10 μM. U937 were treated under the same conditions. Then, the medium was removed and replaced with fresh medium containing 10 μM BCECF-AM. After 30 min, it was fluorescently labeled. U937 cells were washed three times with PBS, supplemented with 1% FBS, and resuspended in endothelial medium. The conditioned medium was removed from HAEC, and labeled U937 (1 mL, 5 × 105 cells) were added and incubated for 120 min at 37°C. Nonadherent monocytes were removed by gentle washing three times with PBS and supplemented with 10% of FBS. Then, 500 μL of lysis buffer (Tris buffer [pH 7.6] and 1% SDS) was added, and fluorescence intensity was measured (485-nm excitation and 520–560-nm emission) using a microplate reader.

Real-Time PCR. To analyze the gene expression, total RNA was isolated from RAW264.7 or U937 cells using the TRIzol reagent according to the manufacturer's specifications (Life Technologies,

Carlsbad CA). Total RNA was further purified using Direct-zol™ RNA MiniPrep (Zymo Research, Irvine, CA), which includes an on-column DNase I treatment. The Zymo-Spin™ IIC Columns were included in the kit. After purification from genomic DNA by DNase-I treatment (Thermo Fisher Scientific, Waltam, MA), 1 μg of RNA from each sample was reverse-transcribed using random hexamer primers with Superscript-II (Thermo Fisher Scientific, Waltam, MA) in a 20 μL reaction volume; 10 ng cDNA were amplified in a 20 μL solution containing 200 nM of each primer and 10 μL of SYBR Select Master Mix (Thermo Fisher Scientific, Waltam, MA). All reactions were performed in triplicate using a Step One Plus machine (Applied Biosystem, Foster City CA). Primers were designed using the software PRIMER3 (https://bioinfo.ut.ee/primer3-0.4.0/) using published data obtained from the NCBI database. For the RAW264.7 murine cell line we used the following primers (forward and reverse): Tnf-α (for CCACCACGCTCTTCTGTCTA; rev AGGGTCTGGGCCATAGAACT), Il-1β (for GCTGAAAGCTCTCCACCTCA; rev AGGCCACAGGTATTTTGTCG) and Il-10 (for CCCAGAAATCAAGGAGCATT; rev CTCTTCACCTGCT CCACTGC). For the U937 human cell line we used the following primers: Tnf-α (for AGCCCATGTTGTAGCAAACC; rev TGAGGTACAGGCCCTCTGAT), Il-1β (for GTGGCAATGAGGATGACTTG; rev GGAGATTCGTAGCTGGATGC) and Ccl2 (for TAGCAGCCACCTTCATTCCC; rev CTGCACTGAGATCTTCCTATTGG).

Statistical analysis. The ANOVA followed by nonparametric Mann-Whitney U test was used for statistical comparisons (*$P < 0.05$) using the Prism 6.0 software (GraphPad).

Physiochemical properties and pharmacokinetic characterization.

Solubility and LogD Measurements. Each compound was dissolved in DMSO at the concentration of 10 mM. Then, ten microliters of the obtained solution were diluted either in 490 μL of PBS pH 7.4 or MeOH and maintained under agitation at 250 rpm for 24 h at r.t. Tubes were subsequently centrifuged for 5 min at 4000 rpm and 10 microliters of each sample were further diluted in 490 μL of MeOH and analyzed by LC-MS/MS. The ratio of mass signal area obtained in PBS and in organic solvent was then calculated and used to determine the solubility of each compound.

LogD was estimated by dissolving 40 µL of selected compounds in 1960 µL of PBS pH 7.4/Octanol. After shaking the mix for 2 hours at rt, organic and aqueous phases were separated and 10 µl of each phase were withdrawn, diluted in 490 µL of MeOH and analyzed by LC-MSMS. Concentrations of products were determined by mass signal and LogD was calculated as the logarithm of the ratio of compounds concentrations in octanol and PBS.

Metabolic Stability. All incubations were performed under shaking at 37 °C in a final volume of 0.5 mL, containing 50 mM potassium phosphate buffer (pH 7.4), all compounds were tested at the final concentration of 1 µM and 1% DMSO was used as vehicle. For microsomes assay, the incubation mixtures contained 0.15 mg of human liver microsomes (Sigma-Aldrich, St. Louis, MO, USA) 5 mM $MgCl_2$, 1 mM NADPH, 5 mM glucose 6-phosphate, 0.4 U·mL−1 glucose 6-phosphate dehydrogenase. Aliquots were removed at 0, 5, 10, 20, 30, 40, 50, 60 min after microsomes addition. For S9 fraction analysis, the buffer contained 0.15 mg of S9 proteins (Sigma-Aldrich, St. Louis, MO, USA), 0.3 mM NADPH, 5.6 mM glucose-6-phosphate, 0.6 units/ml glucose-6-phosphate dehydrogenase, 5.8 mM UDP-glucuronic acid, 0.05 mM acetyl-CoA, 0.5 mM dithiothreitol, 0.5 mM 3'-phosphoadenosine 5'-phosphosulfate, 1 mM glutathione, 0.2 mM acetyl carnitine, 4 units/mL carnitine acetyl transferase, 0.5 mM glycine, and 0.5 mM taurine and aliquots were removed at 0, 5, 15, 30, 45, 60, 90, 120, 150 min after S9 fraction addition. The reaction was stopped by adding 200 µL of ice-cold acetonitrile to withdrawn aliquots. After two hours, samples were centrifuged for 10 min at 10,000 rpm, and supernatants were subjected to LC-MS/MS analysis.

The slope of the linear regression of the curve obtained reporting the natural logarithm of compound area versus incubation time (−k) was used in the conversion to in vitro $t_{1/2}$ values by $t_{1/2} = -\ln(2)/k$. In vitro intrinsic clearance (Cl_{int} expressed as µL/min/mg) was calculated and expressed as µL/min/mg. The percentage of unmodified compound has been calculated assuming the peak area of the compound at time 0 min as 100%. Testosterone was used as a positive control for microsome and phase I enzymes, and 7-hydroxycoumarin was used as positive control for phase II enzymes.

Computational studies.

Receptors and ligand preparation.

CysLT$_1$R. The crystal structure of the homo sapiens Cysteinyl leukotriene receptor 1 (PDB ID 6rz4)[20] was downloaded from the Protein Data Bank website. The soluble cytochrome b562 fragment, the co-crystallized ligand and water molecules were removed and the residue Gln274 was reconstructed. The missing 2 residues of ECL3 and the missing transmembrane helix 8 (TM8) were modeled using the Modeller 9.2 software package.[57,58] For TM8, the crystallographic structure of CysLT$_2$ (PDB ID 6RZ6)[59] was employed as template and its secondary structure was confirmed using prediction tools PSIpred and Spider3.[60,61] Residues protonation states were assigned in accordance with the most populated ones predicted by the H++ webserver[62] at pH 7.4. The final model was validated via 1 μs long molecular dynamics simulation. The protein was put in a box of size 10x10x12 nm and embedded in a lipid bilayer composed of cholesterol (CHL) and 1-parlmitoyl-2-oleoyl-sn-glycero-3-phosphocholine (POPC) with a 30:70 ratio using the CHARMM-GUI webserver.[63] For solvation, TIP3P water molecules were employed and a 0.150 mM concentration of NaCl was added to reach electrostatic neutrality. The simulation was performed using the Amber *ff14SB* and Lipid 17 force fields with the GROMACS 2020.4 software package.[64,65]

GPBAR1. GPBAR1 homology model reported in D'Amore *et al.*[38] was employed for docking calculations. The receptor was prepared as in Biagioli *et al.*[11]

Both the receptors were treated with the Protein Preparation Wizard[66] tool implemented in Maestro ver. 11.8.[67]

Ligands. 3D structures of **1-15** were built using the Graphical User Graphical User Interface (GUI) of Maestro ver. 11.8.[64] The protonation state of **1-15** at pH 7.4 in water has been calculated using the Epik module.[68] Finally, **1-15** were then minimized using the OPLS 2005 force field through 2500 iteration steps of the Polak-Ribiere Conjugate Gradient (PRCG)[69] algorithm.

Docking calculations. Preliminary docking calculations were performed using Glide and Autodock 4.2[70,71] to reproduce the binding pose of the pranlukast ligand recently co-crystalized with $CysLT_1R$ (PDB ID 6rz4).[20] This redocking step allowed to identify the most suitable parameters and scoring function for docking of **1-15**. Considering the ability to reproduce the pranlukast crystallographic binding pose, Glide was finally employed for the docking calculations. The results were clustered and successively ranked according to the Glide Emodel and the Glide Score. Docking calculations of **1-15** on GPBAR1 were performed using the same approach described in *Biagioli et al.*[11]

In order to consider the ligand induced fit effect on the receptors' binding sites – rearrangement of residue side chains to improve interaction with the ligand -, we performed docking calculations on **5** in both GPBAR1 and $CysLT_1R$ using as structure the centroid of the most populated protein conformation during the MD calculations on the **5**/GPBAR1 and **5**/$CysLT_1R$ complex, respectively.

In detail, the docking procedure was carried out with the Glide software package,[72] using the Standard Precision (SP) algorithm of the GlideScore function[37] and the OPLS 2005 force field.[73] A grid box of $2.5 \times 1.6 \times 1.7$ nm for GPBAR1 receptor and one of $1.6 \times 2.0 \times 1.8$ nm for $CysLT_1R$ centered on the ligand binding cavity were created. A total amount of 100 poses was generated and the conformational sampling of the ligand was enhanced by two times, as reported by the default setting of Glide. Docking conformations of **1-15** were then clustered based on their atomic RMSD. Globally, seven clusters were obtained and, among them, only the conformation included in the most populated cluster with both the Glide Emodel and GlideScore lowest-energy value was considered (Figure 6 and 10).

MD calculations. MDs were performed with GROMACS suite ver. 2020.4,[74] using the Amber *ff14SB*, Lipid 17 and the General Amber Force Field (GAFF) parameters[64,75] for the proteins, lipids and ligands, respectively. Protein/ligand complexes were prepared as previously reported for $CysLT_1R$ and GPBAR1 and embedded in a 30:70 CHL/POPC lipid bilayer of sizes 10x10nm. The resulting membrane was then solvated with TIP3P water and a 0.150 mM concentration of NaCl

into a 10x10x12 nm box. The whole procedure was carried on using the CHARMM-GUI webserver.[63] The systems were minimized using the steepest descent algorithm in a two steps procedure. First, the protein and ligand heavy atoms were restrained, whereas water molecules and ions were left free and only the movement on the Z axis of hydroxyl group of CHL and the phosphate group of POPC was restrained. Afterward, the restraints were removed, and a second round of minimization was performed. The systems were then gradually heated from 50 to 300 K using a stepwise approach of NVT/NPT simulations at fixed temperature, before increasing it by 50 K. Each NVT/NPT step lasted 1 ns. An initial restraint of 1000 kJ/mol at 50 K was applied on proteins, ligands and lipids as described for the minimization procedure. After each NVT/NPT cycle, the restraints were lowered by 160 kJ/mol. The Langevin dynamics integrator and the Berendsen barostat with semi-isotropic coupling at 1 atm were employed. After reaching 300 K, a preliminary production run of 10ns without restraints was performed using the Langevin dynamics integrator and the Parrinello-Rahman barostat with semi-isotropic coupling at 1 atm. The same parameters were employed for the following production runs of 1 μs. In all these simulations, a time step integration of 2 fs. For the computation of electrostatic and Van der Waals interactions, the Particle-Mesh Ewald (PME) and the cutoff algorithms were used, respectively, with a threshold of 1.2 nm. The cluster analysis trajectory was carried out using the GROMACS gmx cluster tools with the GROMOS method[76] and a 0.2 nm cutoff.

Free-energy calculations. Well-tempered MetaD simulations were performed using the same protocol described for MD calculations. However, the GROMACS suite ver. 2020.4 was patched with the Plumed software package ver. 2.6.2 and the Cα atoms of the protein structured parts (i.e. alpha helices, beta strands) were restrained around the initial conformation using a RMSD-based harmonic potential with constant 10000 kJ/mol and threshold 0.1 nm. As collective variable, the distance between the heavy atoms of the quinoline moiety and the C_β of $CysLT_1R$ $Arg79^{2.60}$ was chosen. This distance CV was allowed to explore the values from 0 to 3.0 nm to limit the sampling

of the free-energy landscape to the interior of the binding pocket. To do so, an upper wall with constant 10000 kJ/mol was placed at 3.0 nm of the distance CV to prevent the ligand from exiting the $CysLT_1R$ cavity. A bias of 1 kJ/mol was deposited every 5 ps with a sigma of 0.05 nm and a bias factor of 15. The MetaD simulations were performed using 10 multiple walkers lasting 150 ns each, for a total of 1.5 μs of calculation.

MD trajectories were visualized using VMD software[77] and all figures were rendered by UCSF Chimera.[78]

Supporting Information Available. This material is available free of charge via the Internet at http://pubs.acs.org.

- Molecular formula strings for all final compounds (CSV)
- Docking model for **5** and **6** in GPBAR1 and $CysLT_1R$ (PDB)
- Docking model of pranlukast in $CysLT_1R$ (PDB)
- Molecular Dynamics and Metadynamics binding mode of **5** in $CysLT_1R$ (PDB)
- Docking model for **14** in GPBAR1 (PDB)
- Docking model for REV5901 (R and S) in GPBAR1 and $CysLT_1R$ (PDB)
- Docking model for DCA in GPBAR1 (PDB)
- ^{1}H and ^{13}C NMR spectral data for compounds **1-15** and HPLC traces for compounds **5, 6** and **14**; LPS-induced RNA expression in RAW macrophages assay; binding mode of compound **6** superimposed to the binding mode of pranlukast; docking studies of REV5901 (R- and S-OH conformations) in GPBAR1 and $CysLT_1R$ and of DCA in GPBAR1 (PDF)

Author Contributions

V.S., G.B., P.R. and A.Z. designed and performed synthesis; R.R., S.M., M.B., and S.F. designed and performed pharmacological experiments; C.C. designed and performed MS experiments; B.F.,

P.C, B.C. and V.L. designed and performed the computational study, analyzed and interpreted the data. All the authors contributed to manuscript writing and approved the final version.

Notes:

The authors declare the following competing financial interest(s): S.F. and A.Z. have filed the Italian patent application no. 102020000019210 and the corresponding PCT (PCT/IB2021/057131) in the name of PRECISION BIO-THERAPEUTICS S.R.L., a spinoff of the University of Perugia, on same the compounds described in this paper.

Acknowledgements. This work was partially supported by grant from the Italian MIUR/PRIN 2017 (2017FJZZRC). V.L. acknowledges the support from the European Research Council (ERC) (Grant agreement No. 101001784) and the Swiss National Supercomputing Center (CSCS) (project ID u8).

Abbreviations.

$CysLT_1R$, Cysteinyl Leukotriene Receptor 1; DIBAL-H, Diisobutylaluminium hydride; GPCRs, G-Protein Coupled Receptors; GPBAR1, G-Protein coupled Bile Acid Receptor 1; Il-1β and Il-10, interleukin 1β and 10; LTR Leukotriene receptors; LTB4-R1, leukotriene B4 receptor 1; OXER1, Oxoeicosanoid receptor 1; TLCA, taurolithocholic acid; Tnfα, Tumor necrosis factor alpha.

References

(1) Nothacker, H. P.; Wang, Z.; Zhu, Y.; Reinscheid, R. K.; Lin, S. H.; Civelli, O. Molecular cloning and characterization of a second human cysteinyl leukotriene receptor: discovery of a subtype selective agonist. *Mol. Pharmacol.,* **2020**, *58*, 1601-1608.

(2) Yokomizo, T.; Nakamura, M.; Shimizu, T. Leukotriene receptors as potential therapeutic targets. *J. Clin. Invest.* **2018**, *128*, 2691-2701.

(3) Colazzo, F.; Gelosa, P.; Tremoli, E.; Sironi, L.; Castiglioni, L. Role of the cysteinyl leukotrienes in the pathogenesis and progression of cardiovascular diseases. *Mediators Inflamm.* **2017**, 2432958.

(4) Singh, R. K.; Gupta, S.; Dastidar, S.; Ray A. Cysteinyl leukotrienes and their receptors: molecular and functional characteristics. *Pharmacology*, **2010**, *85*, 336-349.

(5) Claesson, H. E.; Dahlen S. E. Asthma and leukotrienes: antileukotrienes as novel anti-asthmatic drugs. *J. Int. Med.*, **1999**, *245*, 205-227.

(6) Drazen, J. M.; Israel, E.; O'Byrne, P. M. Treatment of asthma with drugs modifying the leukotriene pathway. *N. Engl. J. Med.*, **1999**, *340*, 197-206.

(7) Haberal, I.; Corey J. P. The role of leukotrienes in nasal allergy. *Otolaryngol. Head Neck Surg*., **2003**, *129*, 274-279.

(8) Zhang, J.; Migita, O.; Koga, M.; Shibasaki, M.; Arinami, T.; Noguchi, E. Determination of structure and transcriptional regulation of CYSLTR1 and an association study with asthma and rhinitis. *Pediatr. Allergy Immunol.,* **2006**, *17*, 242-249.

(9) Singh, R. K.; Tandon, R.; Dastidar, S. G.; Ray, A. A review on leukotrienes and their receptors with reference to asthma. *The Journal of Asthma*, **2013**, *50*, 922–931.

(10) Capra V. Molecular and functional aspects of human cysteinyl leukotriene receptors. *Pharmacol Res.,* **2004**, *50*, 1-11.

(11) Biagioli, M.; Carino, A.; Marchianò, S.; Roselli, R.; Di Giorgio, C.; Bordoni, M.; Fiorucci, C.; Sepe, V.; Conflitti, P.; Limongelli, V.; Distrutti, E.; Baldoni, M.; Zampella, A.; Fiorucci, S. Identification of cysteinyl-leukotriene-receptor 1 antagonists as ligands for the bile acid receptor GPBAR1. *Biochem. Pharmacol,* **2020,** *177*, 113987.

(12) Duboc, H.; Tache, Y.; Hofmann, A. F. The bile acid TGR5 membrane receptor: from basic research to clinical application. *Dig. Liver Dis.*, **2014**, *46*, 302-312.

(13) Fiorucci, S.; Distrutti, E. Bile acid-activated receptors, intestinal microbiota, and the treatment of metabolic disorders. *Trends Mol. Med.*, **2015**, *21*, 702-714.

(14) Fiorucci, S.; Baldoni, M.; Ricci, P.; Zampella, A.; Distrutti, E.; Biagioli, M. Bile acid-activated receptors and the regulation of macrophages function in metabolic disorders. *Current Opinion in Pharmacology* **2020**, *53*, 45-54.

(15) Fiorucci, S.; Distrutti, E.; Carino, A.; Zampella, A.; Biagioli, M. Bile acids and their receptors in metabolic disorders. *Progress in Lipid Research*. **2021**, *82*, 101094.

(16) De Marino, S.; Finamore, C.; Biagioli, M.; Carino, A.; Marchianò, S.; Roselli, R.; Di Giorgio, C.; Bordoni, M.; Di Leva, F. S.; Novellino, E.; Cassiano, C.; Limongelli, V.; Zampella, A.; Festa, C.; Fiorucci S. GPBAR1 activation by C6-substituted hyodeoxycholane analogues protects against colitis. *ACS Med. Chem. Lett.*, **2020**, *11*, 818-824.

(17) Bellamkonda, K.; Satapathy, S. R.; Douglas, D.; Chandrashekar, N.; Selvanesan, B. C.; Liu, M.; Savari, S.; Jonsson, G.; Sjölander, A. Montelukast, a CysLT1 receptor antagonist, reduces colon cancer stemness and tumor burden in a mouse xenograft model of human colon cancer. *Cancer Lett.*, **2018**, *437*, 13-24.

(18) Watanabe, M.; Houten, S. M.; Mataki, C.; Christoffolete, M. A.; Kim, B. W.; Sato, H.; Messaddeq, N.; Harney, J. W.; Ezaki, O.; Kodama, T.; Schoonjans, K.; Bianco, A. C.; Auwerx, J. Bile acids induce energy expenditure by promoting intracellular thyroid hormone activation. *Nature*, **2006**, *439*, 484-489.

(19) Biagioli, M.; Carino, A.; Cipriani, S.; Francisci, D.; Marchianò, S.; Scarpelli, P.; Sorcini, D.; Zampella, A.; Fiorucci, S. The bile acid receptor GPBAR1 regulates the M1/M2 phenotype of intestinal macrophages and activation of GPBAR1 rescues mice from murine colitis. *J. Immunol.*, **2017**, *199*, 718-733.

(20) Luginina, A.; Gusach, A.; Marin, E.; Mishin, A.; Brouillette, R.; Popov, P.; Shiriaeva, A.; Besserer-Offroy, E.; Longpré, JM; Lyapina, E.; Ishchenko, A.; Patel, N.; Polovinkin, V.; Safronova, N.; Bogorodskiy, A.; Edelweiss, E.; Hu, H.; Weierstall, U.; Liu, W.; Batyuk, A.; Gordeliy, V.; Han, G. W.; Sarret, P.; Katritch, V.; Borshchevskiy, V.; Cherezov, V. Structure-based mechanism of cysteinyl leukotriene receptor inhibition by antiasthmatic drugs. *Sci. Adv.,* **2019,** eaax2518.

(21) Yang, F.; Mao, C.; Guom, L.; Lin, J.; Ming, Q.; Xiao, P.; Wu, X.; Shen, O.; Guo, S.; Shen, D.; Lu, R.; Zhang, L.; Huang, S.; Ping, Y.; Zhang, C.; Ma, C.; Zhang, K.; Liang, X.; Shen, Y.; Nan, F.; Yi, F.; Luca, V. C.; Zhou, J.; Jiang, C.; Sun, J.; Xie, X.; Yu, X.; Zhang, Y. Structural basis of GPBAR activation and bile acid recognition. *Nature*, **2020**, *587*, 499-504.

(22) Chen, G.; Wang, X.; Ge, Y.; Ma, L.; Chen, O.; Liu, H.; Du, Y.; Ye, R. D.; Hu, H.; Ren, R. Cryo-EM structure of activated bile acids receptor TGR5 in complex with stimulatory G protein. *Signal Transduct. Target Ther*., **2020,** *5*, 142.

(23) Sarau, H. M.; Ames, R.S.; Ellis, C.; Elshourbagy, N.; Foley, J. J.; Schmidt, D. B.; Muccitelli, R. M.; Jenkins, O.; Murdock, P. R.; Herrity, N. C.; Halsey, W.; Sathe, G.; Muir, A. I.; Nuthulaganti, P.; Dytko, G. M.; Buckley, P. T.; Wilson, S.; Bergsma, D. J.; Hay, D. W. Identification, molecular cloning, expression and characterization of a cysteinyl leukotriene receptor. *Mol. Pharmacol*., **1999**, *56*, 657-663.

(24) Renga, B.; Cipriani, S.; Carino, A.; Simonetti, M.; Zampella, A.; Fiorucci, S. Reversal of endothelial dysfunction by GPBAR1 agonism in portal hypertension involves a AKT/FOXOA1 dependent regulation of H2S generation and endothelin-1. *PLoS One*., **2015**, *10,* e0141082.

(25) Renga, B.; Bucci, M.; Cipriani, S.; Carino, A.; Monti, M.C.; Zampella, A.; Gargiulo, A.; d'Emmanuele di Villa Bianca, R.; Distrutti, E.; Fiorucci, S. Cystathionine γ-lyase, a H2S-generating

enzyme, is a GPBAR1-regulated gene and contributes to vasodilation caused by secondary bile acids. *Am J Physiol Heart Circ Physiol*., **2015**, *309*, H114-126.

(26) Carino, A.; Marchianò, S.; Biagioli, M.; Bucci, M.; Vellecco, V.; Brancaleone, V.; Fiorucci, C.; Zampella, A.; Monti, M. C.; Distrutti, E.; Fiorucci, S. Agonism for the bile acid receptor GPBAR1 reverses liver and vascular damage in a mouse model of steatohepatitis. *FASEB J*., **2019**, *33*, 2809-2822.

(27) Biagioli, M.; Carino, A.; Fiorucci, C.; Marchianò, S.; Di Giorgio, C.; Bordoni, M.; Roselli, R.; Baldoni, M.; Distrutti, E.; Zampella, A.; Fiorucci, S. The bile acid receptor GPBAR1 modulates CCL2/CCR2 signaling at the liver sinusoidal/macrophage interface and reverses acetaminophen-induced liver toxicity. *J Immunol.*, **2020**, *204*, 2535-2551.

(28) Nagata, M.; Saito, K.; Tsuchiya, K.; Sakamoto, Y. Leukotriene D4 upregulates eosinophil adhesion via the cysteinyl leukotriene 1 receptor. *J Allergy Clin Immunol*., **2002**, *109*, 676-680.

(29) Boehmler, A. M.; Drost, A.; Jaggy, L.; Seitz, G.; Wiesner, T.; Denzlinger, C.; Kanz, L.; Möhle, R. The CysLT1 ligand leukotriene D4 supports alpha4beta1- and alpha5beta1-mediated adhesion and proliferation of CD34+ hematopoietic progenitor cells. *J Immunol*., **2009**, *182*, 6789-6798.

(30) Meliton, A. Y.; Muñoz, N. M.; Osan, C. M.; Meliton, L. N.; Leff, A. R. Leukotriene D4 activates β2-integrin adhesion in human polymorphonuclear leukocytes. *Eur Respir J*., **2010**, *35*, 402-409.

(31) Zhou, X.; Cai, J.; Liu, W.; Wu, X.; Gao, C. Cysteinyl leukotriene receptor type 1 (CysLT1R) antagonist zafirlukast protects against TNF-α-induced endothelial inflammation. *Biomed Pharmacother*., **2019**, *111*, 452-459.

(32) Anzini, M.; Braile, C.; Valenti, S.; Cappelli, A.; Vomero, S.; Marinelli, L.; Limongelli, V.; Novellino, E.; Betti, L.; Giannaccini, G.; Lucacchini, A.; Ghelardini, C.; Norcini, M.; Makovec, F.; Giorgi, G.; Ian Fryer, R. Ethyl 8-fluoro-6-(3-nitrophenyl)-4H-imidazo[1,5-a][1,4]benzodiazepine-3-carboxylate as novel, highly potent, and safe antianxiety agent. *J Med Chem*, **2008**, *51*, 4730-4743.

(33) Anzini, M.; Valenti, S.; Braile, C.; Cappelli, A.; Vomero, S.; Alcaro, S.; Ortuso, F.; Marinelli, L.; Limongelli, V.; Novellino, E.; Betti, L.; Giannaccini, G.; Lucacchini, A.; Daniele, S.; Martini, C.; Ghelardini, C.; Di Cesare Mannelli, L.; Giorgi, G.; Mascia, M. P.; Biggio, G. New insight into the central benzodiazepine receptor-ligand Interactions: design, synthesis, biological evaluation, and molecular modeling of 3-substituted 6-phenyl-4H-imidazo[1,5-a][1,4]benzodiazepines and related compounds. *J. Med. Chem.,* **2011**, *54*, 5694-5711.

(34) Nuti, E.; Casalini, F.; Avramova, S. I.; Santamaria, S.; Fabbi, M.; Ferrini, S.; Marinelli, L.; La Pietra, V.; Limongelli, V.; Novellino, E.; Cercignani, G.; Orlandini, G.; Nencetti, S.; Rossello, A.

Potent arylsulfonamide inhibitors of tumor necrosis factor-alpha converting enzyme able to reduce activated leukocyte cell adhesion molecule shedding in cancer cell models. *J. Med. Chem.*, **2010**, *53*, 2622-2635.

(35) Limongelli, V. Ligand binding free energy and kinetics calculation in 2020. *Wiley Interdiscip. Rev. Comput. Mol*. Sci., **2020**, *10*, e1455.

(36) Halgren, T. A.; Murphy, R. B.; Friesner, R. A.; Beard, H. S.; Frye, L. L.; Pollard, W. T.; Banks, J. L. Glide: a new approach for rapid, accurate docking and scoring. 2. Enrichment factors in database screening. *J. Med. Chem.*, **2004**, *47*, 1750-1759.

(37) Friesner, R. A.; Banks, J. L.; Murphy, R. B.; Halgren, T. A.; Klicic, J. J.; Mainz, D. T.; Repasky, M. P.; Knoll, E. H.; Shelley, M.; Perry, J. K.; Shaw, D. E.; Francis, P.; Shenkin, P. S. Glide: a new approach for rapid, accurate docking and scoring. 1. Method and assessment of docking accuracy. *J. Med. Chem.,* **2004**, *47*, 1739-1749.

(38) D'Amore, C.; Di Leva, F. S.; Sepe, V.; Renga, B.; Del Gaudio, C.; D'Auria, M. V.; Zampella, A.; Fiorucci, S.; Limongelli V. Design, synthesis, and biological evaluation of potent dual agonists of nuclear and membrane bile acid receptors. *J. Med. Chem.,* **2014**, *57*, 937-954.

(39) Di Leva, F. S.; Festa, C.; Carino, A.; De Marino, S.; Marchianò, S.; Di Marino, D.; Finamore, C.; Monti, M. C.; Zampella, A.; Fiorucci, S.; Limongelli, V. Discovery of ((1, 2, 4-oxadiazol-5-yl) pyrrolidin-3-yl) ureidyl derivatives as selective non-steroidal agonists of the G-protein coupled bile acid receptor-1. *Sci. Rep.,* **2019**, *9*, 43290.

(40) De Marino, S.; Carino, A.; Masullo, D.; Finamore, C.; Marachianò, S.; Cipriani, S.; Di Leva, F. S.; Catalanotti, B.; Novellino, E.; Limongelli, V.; Fiorucci, S.; Zampella, A. Hyodeoxycholic acid derivatives as liver X receptor α and G-protein-coupled bile acid receptor agonists. *Sci. Rep.,* **2017**, *7*, 43290.

(41) Sepe, V.; Renga, B.; Festa, C.; D'Amore, C.; Masullo, D.; Cipriani, S.; Di Leva, F. S.; Monti, M. C.; Novellino, E.; Limongelli, V.; Zampella, A.; Fiorucci, S. Modification on ursodeoxycholic acid (UDCA) scaffold. discovery of bile acid derivatives as selective agonists of cell-surface G-protein coupled bile acid receptor 1 (GP-BAR1). *J. Med. Chem.,* **2014**, *57*, 7687-7701.

(42) Di Leva, F. S.; Festa, C.; Renga, B.; Sepe, V.; Novellino, E.; Fiorucci, S.; Zampella, A.; Limongelli, V. Structure-based drug design targeting the cell membrane receptor GPBAR1: exploiting the bile acid scaffold towards selective agonism. *Sci. Rep.*, **2015**, *5*, 16605.

(43) Macchiarulo, A.; Gioiello, A.; Thomas, C.; Pols, T. W. H.; Nuti, R.; Ferrari, C.; Giacchè, N.; De Franco, F.; Pruzanski, M.; Auwerx, J.; Schoonjans, K.; Pellicciari, R. Probing the binding site of bile acids in TGR5. *ACS Med. Chem. Lett.*, **2013**, *4*, 1158-1162.

(44) Ballesteros, J. A.; Weinstein, H. Receptor molecular biology. *Recept. Mol. Biol.* **1995**, *25*, 366-428.

(45) Limongelli, V.; Marinelli, L.; Cosconati, S.; La Motta, C.; Sartini, S.; Mugnaini, L.; Da Settimo, F.; Novellino, E.; Parrinello, M. Sampling protein motion and solvent effect during ligand binding. *Proc. Natl Acad. Sci. USA*, **2012**, *109*, 1467-1472.

(46) Laio, A.; Parrinello, M. Escaping free energy minima. *Proc. Natl Acad. Sci. USA*, **2002**, *99*, 12562–12566.

(47) Barducci, A.; Bussi, G.; Parrinello, M. Well-tempered metadynamics: a smoothly converging and tunable free-energy method. *Phys. Rev. Lett*., **2008**, *100*, 020603.

(48) Casasnovas, R.; Limongelli, V.; Tiwary, P.; Carloni, P.; Parrinello, M. Unbinding kinetics of a p38 MAP kinase type II inhibitor from metadynamics simulations. *J. Am. Chem. Soc.*, **2017**, *139*, 4780–4788.

(49) Moraca, F.; Amato, J.; Ortuso, F.; Artese, A.; Pagano, B.; Novellino, E.; Alcaro, S.; Parrinello, M.; Limongelli, V. Ligand binding to telomeric G-quadruplex DNA investigated by funnel-metadynamics simulations. *Proc. Natl. Acad. Sci. USA*, **2017**, *114*, E2136–E2145.

(50) Limongelli, V.; Bonomi, M.; Parrinello, M. Funnel metadynamics as accurate binding free-energy method. *Proc. Natl. Acad. Sci. USA*, **2013**, *110*, 6358-6363.

(51) Saleh, N.; Ibrahim, P.; Saladino, G.; Gervasio, F. L.; Clark, T. An efficient metadynamics-based protocol to model the binding affinity and the transition state ensemble of G-protein-coupled receptor ligands. *J. Chem. Inf. Model.*, **2017**, *57*, 1210-1217.

(52) Raniolo, S.; Limongelli, V. Ligand binding free-energy calculations with funnel metadynamics. *Nat. Protoc.*, **2020**, *15*, 2837-2866.

(53) Macchiarulo, A.; Gioiello, A.; Thomas, C.; Pols, T.W.H.; Nuti, R.; Ferrari, C.; Giacchè, N.; De Franco, F.; Pruzanski, M.; Auwerx, J.; Schoonjans, K.; Pellicciari, R. Probing the Binding Site of Bile Acids in TGR5. *ACS Med. Chem. Lett.*, **2013**, *4*, 1158-1162.

(54) Knoll, R.; Schultze, J. L.; Schulte-Schrepping, J. Monocytes and macrophages in COVID-19. *Front Immunol.*, **2021**, *12*, 720109.

(55) Belchamber, K. B. R.; Hughes, M. J.; Spittle, D. A.; Walker, E. M.; Sapey, E. New pharmacological tools to target leukocyte trafficking in lung disease. *Front Immunol.*, **2021**, *12*, 704173.

(56) Wiendl, M.; Becker, E.; Müller, T.M.; Voskens, C. J.; Neurath, M. F.; Zundler, S. Targeting immune cell trafficking - insights from research models and implications for future IBD therapy. *Front Immunol.*, **2021**, *12*, 656452.

(57) Webb, B.; Sali, A. Comparative protein structure modeling using MODELLER. *Current Protocols in* Bioinformatics, **2016**, 5.6.1-5.6.37.

(58) Fiser, A.; Do, R. K.; Sali, A. Modeling of loops in protein structures, *Protein Sci.*, **2000**, *9*, 1753-1773.

(59) Gusach, A.; Luginina, A.; Marin, E.; Brouillette, R. L.; Besserer-Offroy, E.; Longpré, JM; Ishchenko, A.; Popov, P.; Patel, N.; Fujimoto, T.; Maruyama, T.; Stauch,B.; Ergasheva, M.; Romanovskaia, D.; Stepko, A.; Kovalev, K.; Shevtsov, M.; Gordeliy, V.; Han, G. W.; Katritch, V.; Borshchevskiy, V.; Sarret, P.; Mishin, A.; Cherezov, V. Structural basis of ligand selectivity and disease mutations in cysteinyl leukotriene receptors. *Nat. Commun*., **2019**, *10*, 5573.

(60) Buchan, D. W. A.; Jones, D. T. The PSIPRED protein analysis workbench: 20 years on. *Nucleic Acids Res.*, **2019**, *47*, W402-W407.

(61) Heffernan, R.; Paliwal, K.; Lyons, J.; Singh, J.; Yang, Y.; Zhou, Y. Single-sequence-based prediction of protein secondary structures and solvent accessibility by deep whole-sequence learning. *J. Comput. Chem*., **2018**, *39*, 2210-2216.

(62) Anandakrishnan, R.; Aguilar, B.; Onufriev, A. V. H++ 3.0: automating pK prediction and the preparation of biomolecular structures for atomistic molecular modeling and simulations. *Nucleic Acids Res.*, **2012**, *40*, W537-W541.

(63) Jo, S.; Kim, T.; Iyer, V. G.; Im, W. CHARMM-GUI: a web-based graphical user interface for CHARMM. *J. Comput. Chem.*, **2008**, *29*, 1859-1865.

(64) Maier, J. A.; Martinez, C.; Kasavajhala, K.; Wickstrom, L.; Hauser, K. E.; Simmerling, C. ff14SB: improving the accuracy of protein side chain and backbone parameters from ff99SB. *J. Chem. Theory Comput.*, **2015**, *11*, 3696-3713.

(65) Abraham, M. J.; Murtulo, T.; Schulz, R.; Páll, S.; Smith, J. C.; Hess, B.; Lindahl, E. GROMACS: high performance molecular simulations through multilevel parallelism from laptops to supercomputers. *SoftwareX*, **2015**, 1–2, 19-25.

(66) Sastry, G. M.; Adzhigirey, M.; Day, T.; Annabhimoju, R.; Sherman, W. Protein and ligand preparation: parameters, protocols, and influence on virtual screening enrichments. *J. Comput. Aided Mol. Des.*, **2013**, *27*, 221-234.

(67) Schrödinger Release 2019-1: Maestro, New York, NY: Schrödinger, LLC, **2019**.

(68) Shelley, J. C.; Cholleti, A.; Frye, L. L.; Greenwood, J. R.; Timlin, M. R.; Uchimaya, M. Epik: a software program for pKa prediction and protonation state generation for drug-like molecules. *J. Comput. Aided Mol. Des.*, **2007**, *21*, 681-691.

(69) Grippo, L.; Lucidi, S. A globally convergent version of the Polak-Ribière conjugate gradient method. *Mathematical Programming*, **1997**, *78*, 375–391.

(70) Huey, R.; Morris, G. M.; Olson, A. J. and Goodsell, D. S. A semiempirical free energy force field with charge-based sesolvation. *J. Comput. Chem.*, **2007**, *28*, 1145-1152.

(71) Morris, G. M.; Huey, R.; Lindstrom, W.; Sanner, M. F.; Belew, R. K.; Goodsell, D. S.; Olson, A. J. Autodock4 and AutoDockTools4: automated docking with selective receptor flexibility. *J. Comput. Chem.*, **2009**, *16*, 2785-2791.

(72) Glide, version 7.1. New York, NY: Schrödinger, LLC, **2019**.

(73) Banks, J. L.; Beard, H. S.; Cao, Y.; Cho, A. E.; Damm, W.; Farid, R.; Felts, A. K.; Halgren, T. A.; Mainz, D. T.; Maple, J. R.; Murphy, R.; Philipp, D. M.; Repasky, M. P.; Zhang, L. Y.; Berne, B. J.; Friesner, R. A.; Gallicchio, E.; Levy, R. M. Integrated modeling program, applied chemical theory (IMPACT). *J. Comput. Chem.*, **2005**, *26*, 1752-1780.

(74) Pronk, S.; Pall, S.; Schulz, R.; Larsson, P.; Bjelkmar, P.; Apostolov, R.; Shirts, M. R. GROMACS 4.5: a high-throughput and highly parallel open source molecular simulation toolkit. *Bioinformatics*, **2013**, *29*, 845-854.

(75) Wang, J.; Wolf, R. M.; Caldwell, J. W.; Kollman, P. A.; Case, D. A. Development and testing of a general Amber force field. *J. Comput. Chem.* **2004**, *25*, 1157-1174.

(76) Daura, X.; van Gunsteren, W. F.; Jaun, B.; Mark, A. E.; Gademann, K.; Seebach, D. Peptide folding: when simulation meets experiment. *Angew. Chemie Int. Ed.* **1999**, *38* (1/2), 236-240.

(77) Humphrey, W.; Dalke, A.; Schulten, K. VMD - visual molecular dynamics. *J. Molec. Graphics* **1996**, 14.1, 33-38.

(78) Pettersen, E. F.; Goddard, T. D.; Huang, C. C.; Couch, G. S.; Greenblatt, D. M.; Meng, E. C.; Ferrin, T. E. UCSF Chimera—a visualization system for exploratory research and analysis. *J. Comput. Chem.* **2004**, *25*, 1605-1612.

Table of Contents graphic